

Barren plateaus in quantum tensor network optimization

Enrique Cervero Martín*

Quantinuum, Partnership House, Carlisle Place, London SW1P 1BX, United Kingdom and
Centre for Quantum Technologies, National University of Singapore, 3 Science Drive 2, Singapore 117543

Kirill Plekhanov and Michael Lubasch†

Quantinuum, Partnership House, Carlisle Place, London SW1P 1BX, United Kingdom

(Dated: September 1, 2022)

We analyze the barren plateau phenomenon in the variational optimization of quantum circuits inspired by matrix product states (qMPS), tree tensor networks (qTTN), and the multiscale entanglement renormalization ansatz (qMERA). We consider as the cost function the expectation value of a Hamiltonian that is a sum of local terms. For randomly chosen variational parameters we show that the variance of the cost function gradient decreases exponentially with the distance of a Hamiltonian term from the canonical centre in the quantum tensor network. Therefore, as a function of qubit count, for qMPS most gradient variances decrease exponentially and for qTTN as well as qMERA they decrease polynomially. We also show that the calculation of these gradients is exponentially more efficient on a classical computer than on a quantum computer.

I. INTRODUCTION

Noisy intermediate-scale quantum (NISQ) devices possess just a small number of imperfect qubits [1] but offer unprecedented computational capabilities. Whilst not powerful enough to run paradigm-shifting quantum algorithms with guaranteed quantum advantage, such as Shor's algorithm [2] or Grover search [3], they can already outperform classical computers [4, 5].

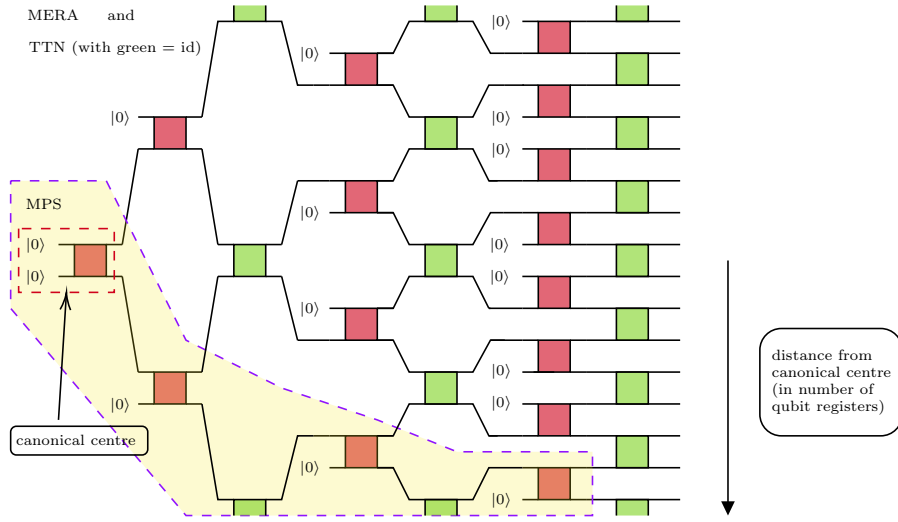


Figure 1: Summary of the main results. We consider the qMERA with periodic boundary conditions (all gates shown; top light green gates connect to bottom ones), the qTTN (dark red gates) and the qMPS (dark red gates in shaded area). For most gates in these circuits the gradient variance with respect to randomly chosen parameters decreases exponentially with the distance of the cost function's observable from the canonical centre. As a function of qubit count this distance can grow linearly for qMPS and it does grow logarithmically for both qTTN and qMERA so that the corresponding gradient variances decrease exponentially and polynomially, respectively.

Variational quantum algorithms are a promising toolbox to work with NISQ devices and achieve a quantum advantage [6–8]. The variational approach is characterized by an iterative feedback loop between a quantum and

* enrique.cervero@u.nus.edu

† michael.lubasch@quantinuum.com

a classical computer during which a parameterized quantum circuit (PQC) is optimized to solve the problem of interest. On the quantum device, the PQC is applied to some initial state to realize the variational wavefunction on which measurements are performed. The measurement results are subsequently processed on the classical device which, e.g., evaluates the cost function, computes gradients and updates the PQC parameters.

Since the seminal articles proposing the variational quantum eigensolver (VQE) [9] and quantum approximate optimization algorithm (QAOA) [10], variational quantum algorithms have been designed and analyzed for numerous applications including combinatorial optimization [11–13], machine learning [14–16], quantum chemistry [17–20], finance [21, 22], partial differential equations [23, 24] and Hamiltonian simulation [25, 26].

The variational optimization of a PQC, however, is hard [27]. One of the difficulties that can be encountered during the optimization is related to the barren plateau phenomenon [28] which manifests itself by a parameter landscape of the cost function that, in simple terms, is flat everywhere except for narrow gorges surrounding local minima. These flat landscapes pose a problem for the optimization of a PQC as they imply that one needs to run the quantum computer and collect samples many times to accurately determine the gradients of the cost function with respect to the variational parameters. The large sampling cost can rule out any quantum advantage one is aiming at with variational quantum algorithms. The severity of the barren plateau problem depends on the cost function [29] and the PQC architecture [28, 30, 31]. A plethora of proposals exist to avoid barren plateaus in certain cases [29, 31–40].

In this article we study the trainability of quantum tensor networks using the approach [31] which is based on the ZX-calculus [41, 42]. Tensor networks have proven to be a powerful variational ansatz for the simulation of quantum many-body systems on classical computers [43–49]. Quantum tensor networks have become popular recently since they can be realized on current NISQ devices [50–56] and have advantages over their classical counterparts [57–59]. We focus on PQC architectures inspired by matrix product states [60–63] (qMPS), tree tensor networks [64–67] (qTTN) and the multiscale entanglement renormalization ansatz [68, 69] (qMERA). An important concept in these tensor networks is the canonical centre which is the first quantum gate of the circuit. We show that the barren plateau phenomenon is fundamentally connected to the distance between the observable of interest and the canonical centre. Figure 1 summarizes our results.

Our analysis is inspired by [31] and extends their results. For the qMPS ansatz considered in [31] we study the barren plateau problem in more detail. In [31] a discriminative qTTN is analyzed and here we explore the corresponding generative variant [67], which represents the quantum counterpart to standard classical TTN [64–67]. Additionally we investigate a qMERA ansatz not considered in [31].

This article is structured as follows. In Sec. II we present the necessary background. Section III contains the results. Technical details including the proofs are provided in appendices.

II. BACKGROUND

We collect background information on VQE in Sec. II A, the barren plateau phenomenon in Sec. II B and the ZX-calculus in Sec. II C

A. Variational quantum eigensolver

Originally introduced in [9] the variational quantum eigensolver (VQE) consists of a training loop that iterates between a quantum and a classical computer and makes use of the variational principle to solve the minimization problem $\langle H \rangle_{\theta^*} = \min_{\theta} \langle H \rangle_{\theta}$ where

$$\langle H \rangle_{\theta} = \langle \psi(\theta) | H | \psi(\theta) \rangle, \quad (1)$$

for some Hermitian observable H , e.g. a Hamiltonian. During each training iteration the quantum computer prepares the variational wavefunction $|\psi(\theta)\rangle = U(\theta)|0\rangle$ via a PQC of the form

$$U(\theta) = \prod_{j=1}^M U_j(\theta_j), \quad (2)$$

where $U_j(\theta_j) = \exp(-i\theta_j V_j/2) W_j$, $\theta_j \in [-\pi, \pi]$, $V_j^2 = I$ and W_j is an unparameterized unitary. The quantum computer is also used to compute cost function gradients via the parameter-shift rule

$$\partial_{\theta_j} \langle H \rangle_{\theta} \equiv \partial_j \langle H \rangle_{\theta} = \frac{1}{2} (\langle H \rangle_{\theta + \frac{\pi}{2} \mathbf{e}_j} - \langle H \rangle_{\theta - \frac{\pi}{2} \mathbf{e}_j}) \quad (3)$$

where \mathbf{e}_j is the j -th unit vector [70, 71]. The classical computer subsequently updates the parameters $\boldsymbol{\theta}$ and then feeds them back to the quantum machine for the next training iteration. The parameters are updated e.g. using the gradient descent procedure:

$$\boldsymbol{\theta} \rightarrow \boldsymbol{\theta} - \eta \nabla_{\boldsymbol{\theta}} \langle H \rangle_{\boldsymbol{\theta}}, \quad (4)$$

where η is the learning rate and $\nabla_{\boldsymbol{\theta}} \langle H \rangle_{\boldsymbol{\theta}}$ denotes the gradient vector. An alternative gradient-based method that has become popular in the context of variational quantum algorithms is the Adam optimizer [72]. A comprehensive review article on VQE is [8].

In this article we focus on k -local Hamiltonians, i.e. sums of observables which act on at most k qubits. One example of a 2-local Hamiltonian is the transverse-field quantum Ising chain:

$$H_{\text{Ising}} = -J \sum_{\langle i,j \rangle} Z_i Z_j - h \sum_i X_i, \quad (5)$$

where J and h are Hamiltonian parameters, $\langle i,j \rangle$ represents adjacent qubits and X (Z) is the Pauli X (Z) matrix. Another example is the Heisenberg model:

$$H_{\text{Heis}} = \frac{1}{4} \sum_{\langle i,j \rangle} X_i X_j + Y_i Y_j + Z_i Z_j. \quad (6)$$

B. Barren plateaus

The barren plateau phenomenon in the variational optimization of quantum circuits was first discussed in [28] and characterized in the following way:

Theorem 1. *Let Eq. (1) be a cost function with an associated parameterized ansatz Eq. (2) acting on N qubits. For some $1 \leq k \leq M$ define*

$$U = U_L U_k U_R \quad (7)$$

for $U_L = \prod_{j < k} U_j(\theta_j)$ and $U_R = \prod_{j > k} U_j(\theta_j)$. Then

- $E[\partial_k \langle H \rangle_{\boldsymbol{\theta}}] = 0$,
- $\text{Var}[\partial_k \langle H \rangle_{\boldsymbol{\theta}}] \in O(c^{-N})$ for $c > 1$ if either U_L , U_R or both form random unitary 2-designs

where $E[\cdot]$ denotes the average value and $\text{Var}[\cdot]$ the variance over randomly chosen parameters.

In simple terms Theorem 1 tells us that the unitary 2-design condition establishes a cost landscape which is nearly flat everywhere (barren plateaus) except for exponentially small regions around minima (narrow gorges). Using Chebyshev's inequality we see that for randomly chosen parameters the probability of obtaining a gradient of magnitude $|\partial_k \langle H \rangle_{\boldsymbol{\theta}}| > \kappa$ vanishes exponentially with qubit count¹:

$$\Pr[|\partial_k \langle H \rangle_{\boldsymbol{\theta}} - E[\partial_k \langle H \rangle_{\boldsymbol{\theta}}]| \geq \kappa] \leq \frac{\text{Var}[\partial_k \langle H \rangle_{\boldsymbol{\theta}}]}{\kappa^2} \in O\left(\frac{c^{-N}}{\kappa^2}\right). \quad (8)$$

The barren plateau phenomenon is a problem for the trainability of PQCs since the computation of exponentially small gradients using standard techniques, such as the parameter-shift rule, requires exponentially many measurements on a quantum computer. Because the computational cost of performing these calculations on a classical computer also scales exponentially with qubit count, a classical approach might be more efficient than a quantum one in which case there is no quantum advantage.

While in [28] it is shown that the onset of the unitary 2-design property is caused by large circuit depth, in [29] the authors show that also the form of the cost function affects the depth at which barren plateaus emerge. More specifically they show that PQC optimization with local cost functions is efficient for depths that scale logarithmically

¹ We use the following notation: $f(N) \in O(g(N))$ if $f(N)$ is asymptotically bounded above by $c \cdot g(N)$ for some $c > 0$, $f(N) \in \Omega(g(N))$ if $f(N)$ is asymptotically bounded below by $c \cdot g(N)$ for some $c > 0$, and $f(N) \in \Theta(g(N))$ if $f(N)$ is asymptotically bounded below by $c_1 \cdot g(N)$ and above by $c_2 \cdot g(N)$ for some $c_1, c_2 > 0$.

with qubit count and transitions into the barren plateau regime when depths scale as $O(\text{poly}(\log(N)))$. PQC training based on global cost functions, however, is shown to always be subject to barren plateaus, even for shallow $O(1)$ depth circuits.

Focusing on local observables the analysis in [29] suggests that the onset of barren plateaus is related to the entanglement in the causal cone of the observable². This is analysed in detail in [36] where the authors show that sufficiently large amounts of entanglement in the quantum circuit are necessary for the emergence of unitary 2-designs and claim that entanglement-induced barren plateaus [33, 34, 73] and barren plateaus for local cost functions are equivalent.

Due to its importance for the field of variational quantum algorithms, the barren plateau problem has been studied in many articles. Some articles have identified PQC architectures that avoid barren plateaus [31, 74] and others propose ways to mitigate the barren plateau problem, e.g. in [32] the authors propose to initialize the circuit with shallow identity gates formed by unitaries and their adjoints, in [35] they advertise a layer-wise learning strategy, in [37] they propose to initialize the PQC using previously trained smaller PQCs, in [38] they propose to use a previously trained qMPS for the PQC initialization, and in [40] the authors claim that the barren plateau problem is solved by choosing the initial parameters from a particular Gaussian distribution.

C. ZX-calculus for barren plateau analysis

In [31] Chen Zhao and Xiao-Shan Gao pioneer the use of the ZX-calculus [41, 42] to analyse the barren plateau phenomenon. They use the following assumption:

Assumption 1. *The parameterized quantum ansatz in Eq. (2) is such that*

1. *each gate U_j in U is from $\{R_X = \exp(-i\theta_j X/2), R_Z = \exp(-i\theta_j Z/2), H, CNOT\}$ where H is the Hadamard gate and $CNOT$ the controlled- X gate,*
2. *each parameter θ_j is uniformly sampled from $[-\pi, \pi]$.*

They show:

Theorem 2. *Let Eq. (1) be a cost function with associated parameterized ansatz (2) for N qubits and under Assumption 1:*

- $E[\partial_j \langle H \rangle_{\theta}] = 0$,
- $Var[\partial_j \langle H \rangle_{\theta}] = \frac{|c|^2}{4^N} \sum_{a_k \in \{T_1, T_2, T_3\}, k \neq j} V_U^{a_1, \dots, a_{j-1}, T_2, a_{j+1}, \dots, a_M}$, where c is a constant, $V_U^{a_1, \dots, a_M}$ is a ZX-diagram and a_1, \dots, a_M , T_1 , T_2 and T_3 are labels defining the ZX-diagram [31].

While Theorem 2 does not immediately tell us whether a specific choice of PQC and cost function leads to barren plateaus, it provides us with a constructive procedure to compute the variance of gradients by evaluating ZX-diagrams. This calculation can be further simplified by turning the ZX-diagram into tensor networks whose contraction directly produces the sought-after variance value. In App. A we explain the ZX-calculus formalism that is relevant for this article and also give a simple example that illustrates step-by-step how one can use this formalism to obtain the tensor network for the gradient variance starting from a PQC and using ZX-diagrams.

III. RESULTS

We present the results on qMPS in Sec. III A, qTTN in Sec. III B and qMERA in Sec. III C. In Sec. III D we compare the quantum and classical computational cost of calculating gradients.

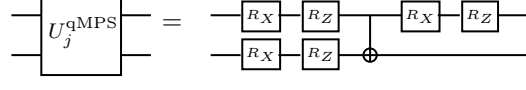
² The causal cone of an observable X_i acting on qubit register i is the sub-circuit composed of only the qubits and gates in the PQC which affect the measurement outcome at site i . If a variational parameter is in the causal cone of an observable then we refer to them as causally connected.

A. Quantum matrix product states

We consider the qMPS ansatz

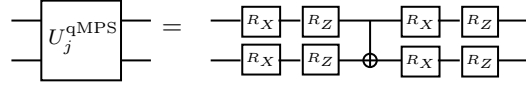
$$U^{\text{qMPS}} := \prod_{j=N-1}^1 U_j^{\text{qMPS}} \quad (9)$$

composed of two-qubit blocks of the form



$$(10)$$

acting on qubits j and $j+1$ for $j < N-1$ and



$$(11)$$

acting on qubits $N-1$ and N , cf. App. B for a full circuit diagram. Here U_1^{qMPS} is the canonical centre of the qMPS.

Theorem 3. *Let $\langle X_i \rangle_{\text{qMPS}}$ be the cost function associated with the observable X_i and consider the qMPS ansatz for N qubits defined in Eq. (9), then:*

$$\text{Var}[\partial_{j,1} \langle X_N \rangle_{\text{qMPS}}] = \begin{cases} \frac{1}{4} \cdot \left(\frac{3}{8}\right)^{N-1} & \text{if } j < N, \\ \frac{1}{4} \left(1 + \left(\frac{3}{8}\right)^{N-1}\right) & \text{if } j = N, \end{cases} \quad (12)$$

$$\text{Var}[\partial_{j,1} \langle X_i \rangle_{\text{qMPS}}] = \begin{cases} 11 \cdot \left(\frac{1}{8}\right)^2 \left(\frac{3}{8}\right)^{i-1} & \text{if } j < i \text{ or } j = i = 1, \\ 3 \cdot \left(\frac{1}{8}\right)^2 \left(1 + \frac{11}{8} \cdot \left(\frac{3}{8}\right)^{i-2}\right) & \text{if } j = i, \\ 3 \cdot \left(\frac{1}{8}\right)^2 \left(1 + \left(\frac{3}{8}\right)^{i-1}\right) & \text{if } j = i + 1, \end{cases} \quad (13)$$

where $\partial_{j,1} \langle X_i \rangle_{\text{qMPS}}$ refers to the gradient w.r.t. the 1-st parameter in the j -th qubit register.

Proof. See App. B, Theorem 7 and Theorem 8. \square

Theorem 3 tells us that the gradient variance with respect to parameter $(j, 1)$ for $j < i$ is independent of j and depends only on i , i.e. the distance between the observable at site i and the canonical centre. We also learn from Theorem 3 that for $j = i, i+1$ the gradient variance has a constant contribution. Note that for $j > i+1$ we have $\text{Var}[\partial_{j,k} \langle X_i \rangle_{\text{qMPS}}] = 0$ since the variational parameter indexed by (j, k) is outside the causal cone of the observable X_i , see e.g. Fig. 4 in App. B. We show in App. B that $\text{Var}[\partial_{j,k} \langle X_i \rangle_{\text{qMPS}}] \geq \text{Var}[\partial_{1,1} \langle X_i \rangle_{\text{qMPS}}]$ for all j, k for which $\text{Var}[\partial_{j,k} \langle X_i \rangle_{\text{qMPS}}] \neq 0$. In other words the variance w.r.t. the top-left parameter is a lower bound to all other non-zero variances in the qMPS ansatz.

According to Theorem 3 Hamiltonians such as the Ising model in Eq. (5) and the Heisenberg model in Eq. (6) do not lead to exponentially vanishing gradients due to the constant contributions in Eq. (13). We see in Theorem 3, however, that for $j < i$ the variance decreases exponentially with i . Therefore if we want to take into account contributions to the gradient by observables acting on sites $i > j$ their calculation suffers from the barren plateau problem. Taking these contributions into account is usually important since the expectation value of a sum of observables (e.g. $\sum_i X_i$) is typically determined on a quantum computer by evaluating the expectation values of the individual observables (X_i) and summing up the results.

Additionally we show:

Theorem 4. *Let $\langle X_i X_{i+1} \rangle_{\text{qMPS}}$ be the cost function associated with the observable $X_i X_{i+1}$ and consider the qMPS ansatz of Eq. (9), then:*

$$\text{Var}[\partial_{1,1} \langle X_i X_{i-1} \rangle_{\text{qMPS}}] = c_i \left(\frac{3}{8}\right)^i, \quad (14)$$

where

$$c_i = \begin{cases} \frac{1}{4} \cdot \left(\left(\frac{3}{8} \right)^2 + \frac{13}{16} \right) & \text{if } i = 1, \\ \frac{1}{4} \cdot \left(\frac{37}{2 \cdot 8^2} + \frac{3}{16} \right) & \text{if } 1 < i < N, \\ \frac{37}{3 \cdot 8^2} & \text{if } i = N - 1, \end{cases} \quad (15)$$

where $\partial_{1,1}\langle X_i \rangle_{qMPS}$ refers to the gradient w.r.t. the 1-st parameter in the 1-st qubit register.

Proof. See App. B, Theorem 9. \square

We generalize the results to k -local observables and propose:

Conjecture 1. If $k \ll N$ then the k -local operators X_I acting on qubits $I = \{i_1, \dots, i_k\}$ with $i_1 < \dots < i_k$ satisfy $\text{Var}[\partial_{1,1}\langle X_I \rangle_{qMPS}] \in \Omega(c^{-i_k})$ for $c > 1$.

The cases $k = 1$ and $k = 2$ are already shown in Theorem 3 and Theorem 4 and we discuss $k > 2$ in App. B.

B. Quantum tree tensor networks

We consider a qTTN ansatz for $N = 2^n$ qubits of the following form for $n = 1$:

$$\begin{array}{c} |0\rangle \xrightarrow{U_{2^1}^{\text{qTTN}}} |0\rangle \\ |0\rangle \xrightarrow{U_{2^1}^{\text{qTTN}}} |0\rangle \end{array} = \begin{array}{c} |0\rangle \xrightarrow{R_X} |0\rangle \xrightarrow{R_Z} |0\rangle \xrightarrow{R_X} |0\rangle \xrightarrow{R_Z} |0\rangle \\ |0\rangle \xrightarrow{R_X} |0\rangle \xrightarrow{R_Z} \oplus |0\rangle \xrightarrow{R_X} |0\rangle \xrightarrow{R_Z} |0\rangle \end{array} \quad (16)$$

and for $n > 1$:

$$\begin{array}{c} |0\rangle^{\otimes 2^{n-1}} \xrightarrow{U_{2^n}^{\text{qTTN}}} |0\rangle^{\otimes 2^{n-1}} \\ |0\rangle^{\otimes 2^{n-1}} \xrightarrow{U_{2^n}^{\text{qTTN}}} |0\rangle^{\otimes 2^{n-1}} \end{array} = \begin{array}{c} |0\rangle^{\otimes 2^{n-1}-1} \xrightarrow{R_X} |0\rangle^{\otimes 2^{n-1}-1} \xrightarrow{R_Z} |0\rangle^{\otimes 2^{n-1}-1} \xrightarrow{U_{2^{n-1}}^{\text{qTTN}}} |0\rangle^{\otimes 2^{n-1}} \\ |0\rangle^{\otimes 2^{n-1}-1} \xrightarrow{R_X} |0\rangle^{\otimes 2^{n-1}-1} \xrightarrow{R_Z} \oplus |0\rangle^{\otimes 2^{n-1}-1} \xrightarrow{U_{2^{n-1}}^{\text{qTTN}}} |0\rangle^{\otimes 2^{n-1}} \end{array} \quad (17)$$

Appendix C contains an example of a full circuit diagram. The top recursion level in Eq. (17) is the canonical centre of the network.

Each qubit in the qTTN ansatz is causally connected to $n = \log N$ qubits, which allows us to show:

Theorem 5. Let $\langle X_i \rangle_{\text{qTTN}}$ be the cost function associated with the observable X_i and consider the qTTN ansatz defined in Eq. (17), then:

1. $\text{Var}[\partial_{1,1}\langle X_1 \rangle_{\text{qTTN}}] \geq \text{Var}[\partial_{1,1}\langle X_i \rangle_{\text{qTTN}}] \geq \text{Var}[\partial_{1,1}\langle X_N \rangle_{\text{qTTN}}]$ for all $i = 1, \dots, N$,
2. $\text{Var}[\partial_{1,1}\langle X_N \rangle_{\text{qTTN}}] = \frac{1}{4} \cdot \left(\frac{3}{8} \right)^n$,
3. $\text{Var}[\partial_{1,1}\langle X_1 \rangle_{\text{qTTN}}] \in \Omega\left(\left(\frac{\lambda_2}{4}\right)^n\right)$ where $\lambda_2 \approx 2.3187$.

Proof. See App. C, Theorem 10 and Lemma 2. \square

In summary Theorem 5 tells us that $\text{Var}[\partial_{1,1}\langle X_i \rangle] \in \Theta(c^{-\log N})$ for all i and for some $c > 1$. We show in App. C that $\text{Var}[\partial_{j,k}\langle X_N \rangle_{\text{qTTN}}] \geq \text{Var}[\partial_{1,1}\langle X_N \rangle_{\text{qTTN}}]$ for all pairs of indices (j, k) provided the former variance is not 0. The variance is 0 in the qTTN ansatz when the variational parameter indexed by (j, k) is outside the causal cone of the observable. In contrast to the qMPS ansatz, for qTTN the variance decreases polynomially and independently of the site i being considered since the distance between the qubit that the observable acts on and the canonical centre is always $\log N$. We conclude that the qTTN ansatz avoids the barren plateau problem.

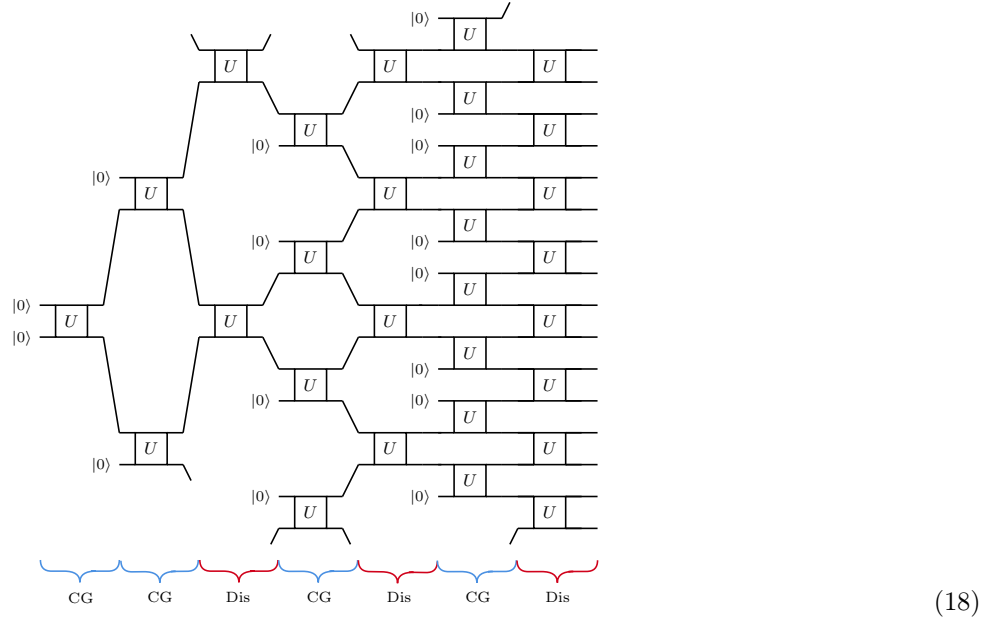
We extend the results to k -local observables for $k \ll N$. In this case the observable is causally connected to $O(k \log N)$ qubits. We propose:

Conjecture 2. If $k \ll N$ then the k -local operators X_I acting on qubits $I = \{i_1, \dots, i_k\}$ satisfy $\text{Var}[\partial_{1,1}\langle X_I \rangle_{\text{qTTN}}] \in \Omega(c^{-k \log N})$.

The case $k = 1$ is covered by Theorem 5 and we discuss the general case in App. C.

C. Quantum multiscale entanglement renormalization ansatz

We define the qMERA ansatz for $N = 2^n$ qubits as a product of n layers each of which is composed of a disentangling (Dis) and a coarse-graining (CG) layer:



where the two qubit gates are given by

$$\begin{array}{c} \text{---} \\ | \\ \text{---} \end{array} \boxed{U} \begin{array}{c} \text{---} \\ | \\ \text{---} \end{array} = \begin{array}{c} \text{---} \\ | \\ \text{---} \end{array} \boxed{R_X} \begin{array}{c} \text{---} \\ | \\ \text{---} \end{array} \boxed{R_Z} \begin{array}{c} \text{---} \\ | \\ \text{---} \end{array} \begin{array}{c} \text{---} \\ | \\ \text{---} \end{array} \quad (19)$$

and in the last layer, prior to the measurements, there is an additional $R_X R_Z$ operation on each qubit register. The canonical centre of the qMERA is in the first CG layer. Each qubit is connected to at most $2 \log N$ qubits via the CG and Dis layers. This quantum tensor network is motivated by the MERA in [69].

Theorem 6. Let $\langle X_i \rangle_{qMERA}$ be the cost function associated with the observable X_i and consider the $qMERA$ ansatz defined in Eq. (18), then:

1. $Var[\partial_{1,1}\langle X_i \rangle_{qMERA}] \geq Var[\partial_{1,1}\langle X_N \rangle_{qMERA}],$
2. $Var[\partial_{1,1}\langle X_N \rangle_{qMERA}] \geq \frac{1}{4} \cdot \left(\frac{3}{8}\right)^{2n}.$

Proof. See App. D.

Theorem 6 tells us that the qMERA avoids barren plateaus for 1-local observables. In contrast to qMPS and qTTN, here the lower bound is not tight. In App. D we present a numerical method to calculate the exact variances. Numerically we find that the upper bound scales as $O(N^{-1.2})$ and the lower bound as $\Omega(N^{-2.7})$.

We extend these results to k -local observables. In this case the observable is causally connected to $O(2k \log N)$ qubits.

Conjecture 3. If $k \ll N$ then the k -local operators X_I acting on qubits $I = \{i_1, \dots, i_k\}$ satisfy $\text{Var}[\partial_{1,1} \langle X_I \rangle_{qMERA}] \in \Omega(c^{-2k} \log N)$.

D. Quantum versus classical computational cost of computing gradients

On a quantum computer we assume that gradients are computed via sampling which has an error scaling as $O(1/\sqrt{M})$ in terms of the sample count M [7]. Therefore, to resolve gradients decreasing exponentially with the distance from the canonical centre, M needs to scale exponentially with that distance.

On a classical computer the computational cost of basic arithmetic operations (addition, subtraction, multiplication and division) scales polynomially with $\log(1/\epsilon)$ for error ϵ [75]. In other words, in classical computing it is efficient to exponentially decrease the error of basic arithmetic operations. For the quantum tensor networks and local observables considered here, gradients can be evaluated on a classical computer via tensor network contraction techniques (see [46] for MPS, [64] for TTN and [69] for MERA). Their computational cost, i.e. the total number of arithmetic operations, scales polynomially with the distance of the observable from the canonical centre and, therefore, the total classical computational cost scales polynomially with that distance.

IV. DISCUSSION

In the context of randomly initialized quantum tensor networks we have shown that qMPS suffer from exponentially vanishing gradients whilst qTTN and qMERA avoid this barren plateau problem. Therefore qTTN and qMERA are recommended over qMPS.

Interestingly any MPS of bond dimension χ can be equivalently represented by a TTN of bond dimension χ^2 [44, 46–49]. Figure 2 illustrates a constructive procedure for transforming a MPS into a TTN (a) and for transforming a qMPS into a qTTN (b) for $N = 8$. The same procedure can be used for larger values of N and, for the qMPS considered in this article, leads to a qTTN composed of four-qubit quantum gates. Since the qTTN circuit depth is logarithmic in the number of qubits the resulting qTTN avoids the barren plateau problem [29].

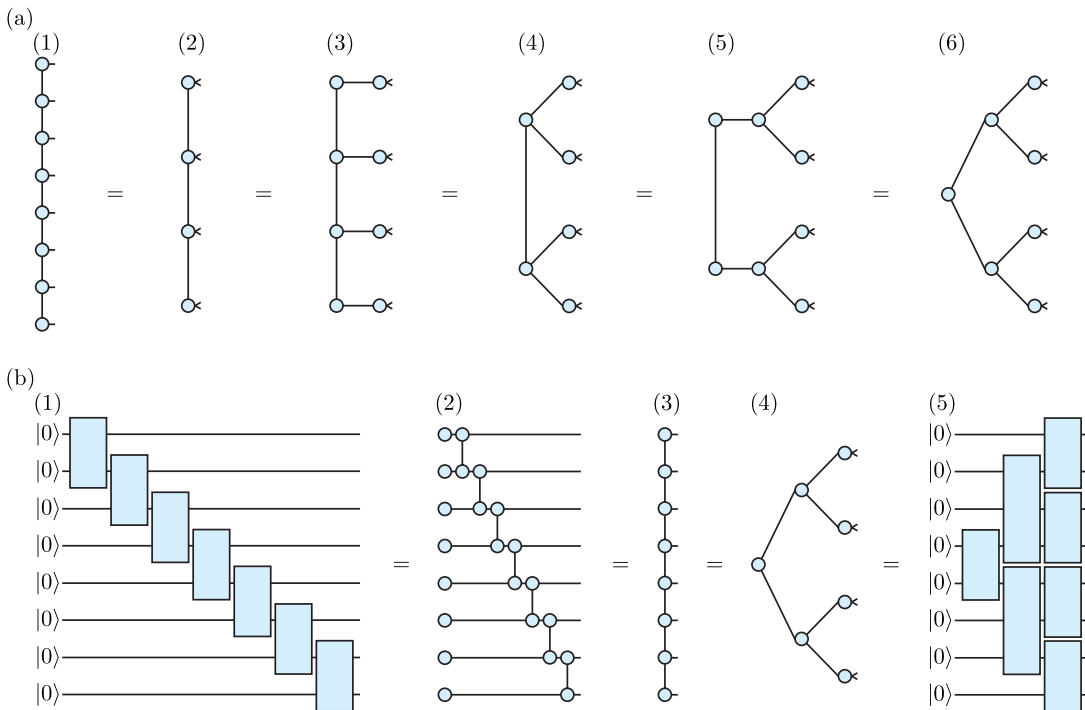


Figure 2: (a) We transform a MPS into a TTN by iterating two steps: 1. We multiply pairs of adjacent tensors, in (1) \rightarrow (2), (3) \rightarrow (4), (5) \rightarrow (6). 2. We perform tensor factorizations, e.g. based on the polar decomposition, in (2) \rightarrow (3), (4) \rightarrow (5). (b) We transform a qMPS into a qTTN in several steps. (1) \rightarrow (2): Tensor factorizations transform the quantum circuit into a tensor network. (2) \rightarrow (3): We multiply adjacent tensors to obtain the MPS. (3) \rightarrow (4): The MPS is turned into a TTN using the procedure in (a). (4) \rightarrow (5): We construct the qTTN from the TTN.

From the perspective of the barren plateau phenomenon, therefore, generalized versions of qTTN and qMERA with larger unitary gates are recommended over qMPS because they can contain qMPS and their depth scales logarithmically with qubit count. We conjecture, however, that the classical computation of gradients for these quantum tensor networks can still be more efficient than their quantum computation, cf. Sec. III D. Our results show that exhausting the possibilities of classical optimization in the context of variational quantum algorithms can have significant advantages, similar to what was also found in other contexts of quantum computation, e.g. Hamiltonian simulation [76, 77].

[1] John Preskill. Quantum computing in the NISQ era and beyond. *Quantum*, 2:79, Aug 2018.

[2] Peter W. Shor. Algorithms for quantum computation: discrete logarithms and factoring. In *Proceedings 35th Annual Symposium on Foundations of Computer Science*, pages 124–134, 1994.

[3] Lov K. Grover. A fast quantum mechanical algorithm for database search. In *Proceedings of the Twenty-Eighth Annual ACM Symposium on Theory of Computing*, STOC ’96, page 212–219, New York, NY, USA, 1996. Association for Computing Machinery.

[4] Frank Arute et al. Quantum supremacy using a programmable superconducting processor. *Nature*, 574(7779):505–510, Oct 2019.

[5] Yulin Wu et al. Strong quantum computational advantage using a superconducting quantum processor. *Physical Review Letters*, 127:180501, Oct 2021.

[6] Marco Cerezo, Andrew Arrasmith, Ryan Babbush, Simon C. Benjamin, Suguru Endo, Keisuke Fujii, Jarrod R. McClean, Kosuke Mitarai, Xiao Yuan, Lukasz Cincio, and Patrick J. Coles. Variational quantum algorithms. *Nature Reviews Physics*, 3(9):625–644, 2021.

[7] Kishor Bharti, Alba Cervera-Lierta, Thi Ha Kyaw, Tobias Haug, Sumner Alperin-Lea, Abhinav Anand, Matthias Degroote, Hermanni Heimonen, Jakob S. Kottmann, Tim Menke, Wai-Keong Mok, Sukin Sim, Leong-Chuan Kwek, and Alán Aspuru-Guzik. Noisy intermediate-scale quantum algorithms. *Reviews of Modern Physics*, 94:015004, Feb 2022.

[8] Jules Tilly et al. The Variational Quantum Eigensolver: a review of methods and best practices. *arXiv:2111.05176*, 2021.

[9] Alberto Peruzzo, Jarrod McClean, Peter Shadbolt, Man-Hong Yung, Xiao-Qi Zhou, Peter J. Love, Alán Aspuru-Guzik, and Jeremy L. O’Brien. A variational eigenvalue solver on a photonic quantum processor. *Nature Communications*, 5(1):4213, Jul 2014.

[10] Edward Farhi, Jeffrey Goldstone, and Sam Gutmann. A quantum approximate optimization algorithm. *arXiv:1411.4028*, 2014.

[11] Leo Zhou, Sheng-Tao Wang, Soonwon Choi, Hannes Pichler, and Mikhail D. Lukin. Quantum approximate optimization algorithm: Performance, mechanism, and implementation on near-term devices. *Physical Review X*, 10:021067, Jun 2020.

[12] David Amaro, Carlo Modica, Matthias Rosenkranz, Mattia Fiorentini, Marcello Benedetti, and Michael Lubasch. Filtering variational quantum algorithms for combinatorial optimization. *Quantum Science and Technology*, 7(1):015021, 2022.

[13] David Amaro, Matthias Rosenkranz, Nathan Fitzpatrick, Koji Hirano, and Mattia Fiorentini. A case study of variational quantum algorithms for a job shop scheduling problem. *EPJ Quantum Technology*, 9(1):5, 2022.

[14] Marcello Benedetti, Erika Lloyd, Stefan Sack, and Mattia Fiorentini. Parameterized quantum circuits as machine learning models. *Quantum Science and Technology*, 4(4):043001, Nov 2019.

[15] Maria Schuld, Alex Bocharov, Krysta M. Svore, and Nathan Wiebe. Circuit-centric quantum classifiers. *Physical Review A*, 101:032308, Mar 2020.

[16] Marcello Benedetti, Brian Coyle, Mattia Fiorentini, Michael Lubasch, and Matthias Rosenkranz. Variational inference with a quantum computer. *Physical Review Applied*, 16:044057, Oct 2021.

[17] Abhinav et al. Kandala. Hardware-efficient variational quantum eigensolver for small molecules and quantum magnets. *Nature*, 549(7671):242–246, Sep 2017.

[18] Yudong Cao et al. Quantum chemistry in the age of quantum computing. *Chemical Reviews*, 119(19):10856–10915, Oct 2019.

[19] Sam McArdle, Suguru Endo, Alán Aspuru-Guzik, Simon C. Benjamin, and Xiao Yuan. Quantum computational chemistry. *Reviews of Modern Physics*, 92:015003, Mar 2020.

[20] Bela Bauer, Sergey Bravyi, Mario Motta, and Garnet Kin-Lic Chan. Quantum algorithms for quantum chemistry and quantum materials science. *Chemical Reviews*, 120(22):12685–12717, 2020. PMID: 33090772.

[21] Kirill Plekhanov, Matthias Rosenkranz, Mattia Fiorentini, and Michael Lubasch. Variational quantum amplitude estimation. *Quantum*, 6:670, Mar 2022.

[22] Dylan Herman, Cody Googin, Xiaoyuan Liu, Alexey Galda, Ilya Safro, Yue Sun, Marco Pistoia, and Yuri Alexeev. A survey of quantum computing for finance. *arXiv:2201.02773*, 2022.

[23] Michael Lubasch, Jaewoo Joo, Pierre Moinier, Martin Kiffner, and Dieter Jaksch. Variational quantum algorithms for nonlinear problems. *Phys. Rev. A*, 101:010301, Jan 2020.

[24] Oleksandr Kyriienko, Annie E. Paine, and Vincent E. Elfving. Solving nonlinear differential equations with differentiable quantum circuits. *Phys. Rev. A*, 103:052416, May 2021.

[25] Xiao Yuan, Suguru Endo, Qi Zhao, Ying Li, and Simon C. Benjamin. Theory of variational quantum simulation. *Quantum*, 3:191, Oct 2019.

[26] Marcello Benedetti, Mattia Fiorentini, and Michael Lubasch. Hardware-efficient variational quantum algorithms for time evolution. *Phys. Rev. Research*, 3:033083, Jul 2021.

[27] Lennart Bittel and Martin Kliesch. Training variational quantum algorithms is NP-hard. *Physical Review Letters*, 127:120502, Sep 2021.

[28] Jarrod R. McClean, Sergio Boixo, Vadim N. Smelyanskiy, Ryan Babbush, and Hartmut Neven. Barren plateaus in quantum neural network training landscapes. *Nature Communications*, 9(1):4812, Nov 2018.

[29] Marco Cerezo, Akira Sone, Tyler Volkoff, Lukasz Cincio, and Patrick J. Coles. Cost function dependent barren plateaus in shallow parametrized quantum circuits. *Nature Communications*, 12(1):1791, Mar 2021.

[30] Arthur Pesah, Marco Cerezo, Samson Wang, Tyler Volkoff, Andrew T. Sornborger, and Patrick J. Coles. Absence of

Barren Plateaus in Quantum Convolutional Neural Networks. *Physical Review X*, 11:041011, Oct 2021.

[31] Chen Zhao and Xiao-Shan Gao. Analyzing the barren plateau phenomenon in training quantum neural networks with the ZX-calculus. *Quantum*, 5:466, Jun 2021.

[32] Edward Grant, Leonard Wossnig, Mateusz Ostaszewski, and Marcello Benedetti. An initialization strategy for addressing barren plateaus in parametrized quantum circuits. *Quantum*, 3:214, Dec 2019.

[33] Carlos Ortiz Marrero, Mária Kieferová, and Nathan Wiebe. Entanglement induced barren plateaus. *arXiv:2010.15968*, 2020.

[34] Joonho Kim and Yaron Oz. Entanglement diagnostics for efficient quantum computation. *arXiv:2102.12534*, 2021.

[35] Andrea Skolik, Jarrod R. McClean, Masoud Mohseni, Patrick van der Smagt, and Martin Leib. Layerwise learning for quantum neural networks. *Quantum Machine Intelligence*, 3(1), Jan 2021.

[36] Stefan H. Sack, Raimel A. Medina, Alexios A. Michailidis, Richard Kueng, and Maksym Serbyn. Avoiding barren plateaus using classical shadows. *PRX Quantum*, 3(2), Jun 2022.

[37] Huan-Yu Liu, Tai-Ping Sun, Yu-Chun Wu, Yong-Jian Han, and Guo-Ping Guo. A parameter initialization method for variational quantum algorithms to mitigate barren plateaus based on transfer learning. *arXiv:2112.10952*, 2021.

[38] James Dborin, Fergus Barratt, Vinul Wimalaweera, Lewis Wright, and Andrew G. Green. Matrix product state pre-training for quantum machine learning. *arXiv:2106.05742*, 2021.

[39] Zidu Liu, Li-Wei Yu, L. M. Duan, and Dong-Ling Deng. The Presence and Absence of Barren Plateaus in Tensor-network Based Machine Learning. *arXiv:2108.08312*, Aug 2021.

[40] Kaining Zhang, Min-Hsueh Hsieh, Liu Liu, and Dacheng Tao. Gaussian initializations help deep variational quantum circuits escape from the barren plateau. *arXiv:2203.09376*, 2022.

[41] Bob Coecke and Ross Duncan. Interacting quantum observables. In Luca Aceto, Ivan Damgård, Leslie Ann Goldberg, Magnús M. Halldórsson, Anna Ingólfssdóttir, and Igor Walukiewicz, editors, *Automata, Languages and Programming*, pages 298–310, Berlin, Heidelberg, 2008. Springer Berlin Heidelberg.

[42] Bob Coecke and Ross Duncan. Interacting quantum observables: categorical algebra and diagrammatics. *New Journal of Physics*, 13(4):043016, Apr 2011.

[43] Ulrich Schollwöck. The density-matrix renormalization group. *Reviews of Modern Physics*, 77:259–315, Apr 2005.

[44] Frank Verstraete, Valentín Murg, and J. Ignacio Cirac. Matrix product states, projected entangled pair states, and variational renormalization group methods for quantum spin systems. *Advances in Physics*, 57(2):143–224, 2008.

[45] Ulrich Schollwöck. The density-matrix renormalization group in the age of matrix product states. *Annals of Physics*, 326(1):96–192, 2011. January 2011 Special Issue.

[46] Román Orús. A practical introduction to tensor networks: Matrix product states and projected entangled pair states. *Annals of Physics*, 349:117–158, 2014.

[47] Román Orús. Tensor networks for complex quantum systems. *Nature Reviews Physics*, 1(9):538–550, 2019.

[48] J. Ignacio Cirac, David Pérez-García, Norbert Schuch, and Frank Verstraete. Matrix product states and projected entangled pair states: Concepts, symmetries, theorems. *Reviews of Modern Physics*, 93:045003, Dec 2021.

[49] Mari Carmen Bañuls. Tensor Network Algorithms: a Route Map. *arXiv:2205.10345*, 2022.

[50] Eli Chertkov et al. Holographic dynamics simulations with a trapped ion quantum computer. *arXiv:2105.09324*, 2021.

[51] Daoheng Niu, Reza Haghshenas, Yuxuan Zhang, Michael Foss-Feig, Garnet Kin-Lic Chan, and Andrew C. Potter. Holographic simulation of correlated electrons on a trapped ion quantum processor. *arXiv:2112.10810*, 2021.

[52] Sajant Anand, Johannes Haensch, Yuxuan Zhang, Andrew C. Potter, and Michael P. Zaletel. Holographic quantum simulation of entanglement renormalization circuits. *arXiv:2203.00886*, 2022.

[53] Adam Smith, Bernhard Jobst, Andrew G. Green, and Frank Pollmann. Crossing a topological phase transition with a quantum computer. *Physical Review Research*, 4:L022020, Apr 2022.

[54] Foss-Feig et al. Entanglement from Tensor Networks on a Trapped-Ion Quantum Computer. *Physical Review Letters*, 128:150504, Apr 2022.

[55] Yuxuan Zhang, Shahin Jahanbani, Daoheng Niu, Reza Haghshenas, and Andrew C. Potter. Qubit-efficient simulation of thermal states with quantum tensor networks. *arXiv:2205.06299*, 2022.

[56] Michael L. Wall, Paraj Titum, Gregory Quiroz, Michael Foss-Feig, and Kaden R. A. Hazzard. Tensor-network discriminator architecture for classification of quantum data on quantum computers. *Physical Review A*, 105:062439, Jun 2022.

[57] William Huggins, Piyush Patil, Bradley Mitchell, K Birgitta Whaley, and E Miles Stoudenmire. Towards quantum machine learning with tensor networks. *Quantum Science and Technology*, 4(2):024001, Jan 2019.

[58] Jin-Guo Liu, Yi-Hong Zhang, Yuan Wan, and Lei Wang. Variational quantum eigensolver with fewer qubits. *Physical Review Research*, 1:023025, Sep 2019.

[59] Michael Foss-Feig et al. Holographic quantum algorithms for simulating correlated spin systems. *Physical Review Research*, 3:033002, Jul 2021.

[60] Mark Fannes, Bruno Nachtergaele, and Reinhard. F. Werner. Finitely correlated states on quantum spin chains. *Communications in Mathematical Physics*, 144(3):443–490, 1992.

[61] Christian Schön, Enrique Solano, Frank Verstraete, Jose I. Cirac, and Michael M. Wolf. Sequential generation of entangled multiqubit states. *Physical Review Letters*, 95:110503, Sep 2005.

[62] David Perez-Garcia, Frank Verstraete, Michael M. Wolf, and J. Ignacio Cirac. Matrix product state representations. *Quantum Info. Comput.*, 7:401, 2007.

[63] Ivan V. Oseledets. Tensor-train decomposition. *SIAM Journal on Scientific Computing*, 33(5):2295–2317, 2011.

[64] Yaoyun Shi, Luming Duan, and Giuseppe Vidal. Classical simulation of quantum many-body systems with a tree tensor network. *Physical Review A*, 74:022320, Aug 2006.

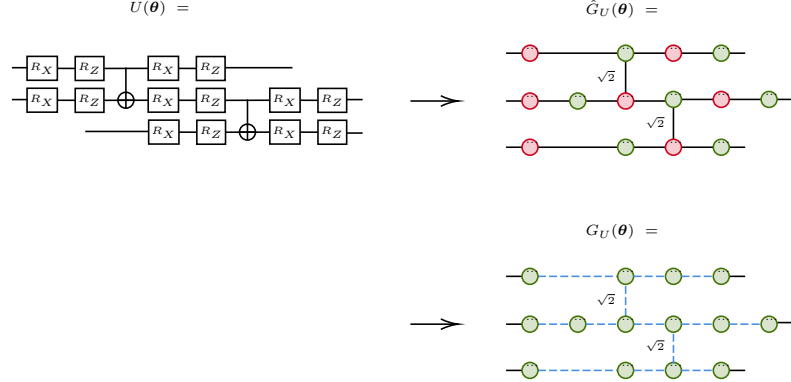
- [65] Wolfgang Hackbusch and Stefan Kühn. A new scheme for the tensor representation. *Journal of Fourier Analysis and Applications*, 15(5):706–722, Oct 2009.
- [66] Luca Tagliacozzo, Glen Evenbly, and Guifre Vidal. Simulation of two-dimensional quantum systems using a tree tensor network that exploits the entropic area law. *Physical Review B*, 80:235127, Dec 2009.
- [67] William Huggins, Piyush Patil, Bradley Mitchell, K Birgitta Whaley, and E Miles Stoudenmire. Towards quantum machine learning with tensor networks. *Quantum Science and technology*, 4(2):024001, 2019.
- [68] Guifre Vidal. Class of quantum many-body states that can be efficiently simulated. *Physical Review Letters*, 101:110501, Sep 2008.
- [69] Glen Evenbly and Guifre Vidal. Algorithms for entanglement renormalization. *Physical Review B*, 79(14), Apr 2009.
- [70] Kosuke Mitarai, Makoto Negoro, Masahiro Kitagawa, and Keisuke Fujii. Quantum circuit learning. *Physical Review A*, 98:032309, Sep 2018.
- [71] Maria Schuld, Ville Bergholm, Christian Gogolin, Josh Izaac, and Nathan Killoran. Evaluating analytic gradients on quantum hardware. *Physical Review A*, 99:032331, Mar 2019.
- [72] Diederik P. Kingma and Jimmy Ba. Adam: A Method for Stochastic Optimization. *arXiv:1412.6980*, Dec 2014.
- [73] Samson Wang, Enrico Fontana, Marco Cerezo, Kunal Sharma, Akira Sone, Lukasz Cincio, and Patrick J. Coles. Noise-induced barren plateaus in variational quantum algorithms. *Nature Communications*, 12(1):6961, Nov 2021.
- [74] Arthur Pesah, Marco Cerezo, Samson Wang, Tyler Volkoff, Andrew T. Sornborger, and Patrick J. Coles. Absence of barren plateaus in quantum convolutional neural networks. *Physical Review X*, 11:041011, Oct 2021.
- [75] Donald E. Knuth. *The Art of Computer Programming, Volume 2: Seminumerical Algorithms, 3rd Edition*. Addison-Wesley Professional, 1997.
- [76] Refik Mansuroglu, Timo Eckstein, Ludwig Nützel, Samuel A. Wilkinson, and Michael J. Hartmann. Variational Hamiltonian simulation for translational invariant systems via classical pre-processing. *arXiv:2106.03680*, 2021.
- [77] Conor Mc Keever and Michael Lubasch. Classically optimized Hamiltonian simulation. *arXiv:2205.11427*, 2022.

Appendix A: ZX-calculus

For the sake of completeness, here we summarise the techniques of [31] that are relevant for our work.

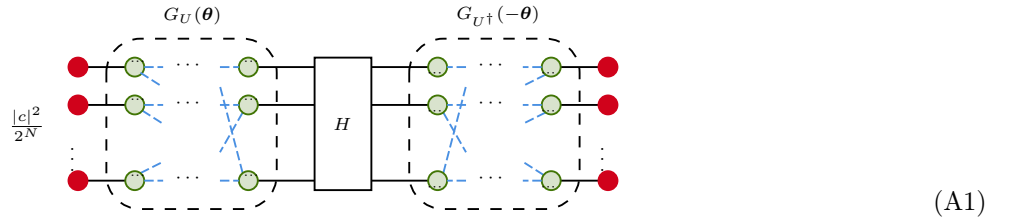
Let $U(\boldsymbol{\theta})$ be a PQC satisfying the constraints of Assumption 1 with $\boldsymbol{\theta} \in [-\pi, \pi]^M$. Then $U(\boldsymbol{\theta}) = c \cdot G_U(\boldsymbol{\theta})$ where $G_U(\boldsymbol{\theta})$ is a graph-like ZX-diagram³ representing the circuit $U(\boldsymbol{\theta})$ and c is the constant obtained in the process of turning $U(\boldsymbol{\theta})$ into $G_U(\boldsymbol{\theta})$.

For example the graph-like ZX-diagram for the 3-qubit qMPS in Eq. (9) is



where the intermediate step $\hat{G}_U(\boldsymbol{\theta})$ corresponds to the usual ZX-diagram with the parameters of the Z and X spiders given implicitly and the blue dashed lines in the last step are Hadamard edges.

Thus for a general PQC and $G_U(\boldsymbol{\theta})$ the quantity $\langle H \rangle_{\boldsymbol{\theta}} := \langle \mathbf{0} | U^\dagger(\boldsymbol{\theta}) H U(\boldsymbol{\theta}) | \mathbf{0} \rangle$ is given by the ZX-diagram

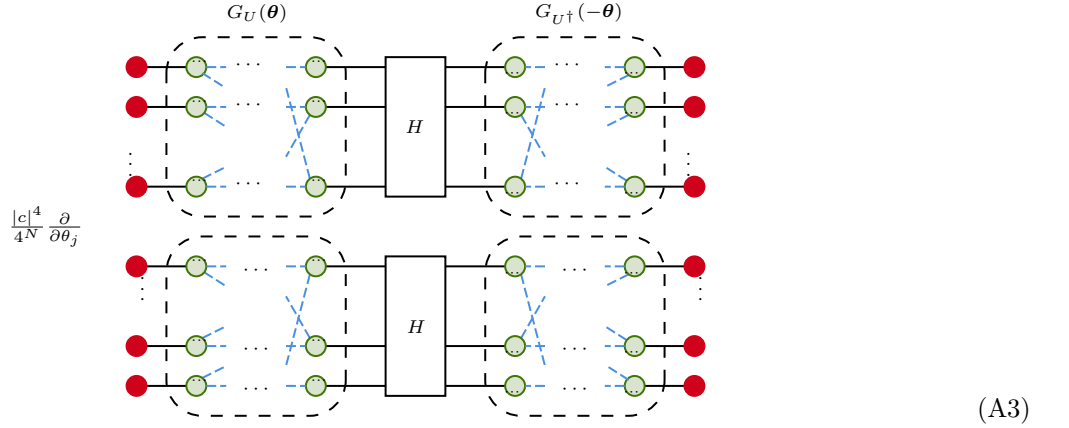


where the prefactor $\frac{1}{2^N}$ comes from the identity $\sqrt{2} |0\rangle = \bullet$.

If we initialise the parameters in the quantum circuit uniformly at random $[-\pi, \pi]^M \leftarrow \boldsymbol{\theta}$, then the variance of the gradient with respect to parameter j is

$$\text{Var} [\partial_j \langle H \rangle_{\boldsymbol{\theta}}] = \frac{1}{(2\pi)^M} \int_{\theta_1} \dots \int_{\theta_M} |\partial_j \langle H \rangle|^2 d\theta_1 \dots d\theta_M \quad (\text{A2})$$

where the integrand is given by

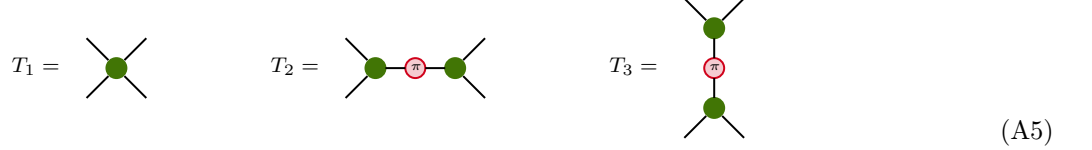


³ A graph-like ZX-diagram is composed entirely of so-called Z spiders connected via non-parallel Hadamard edges, without self-loops, in which every input or output is connected to a Z spider and in which every Z spider is connected to at most one input or output (see [31] for a nice introduction to the ZX-calculus).

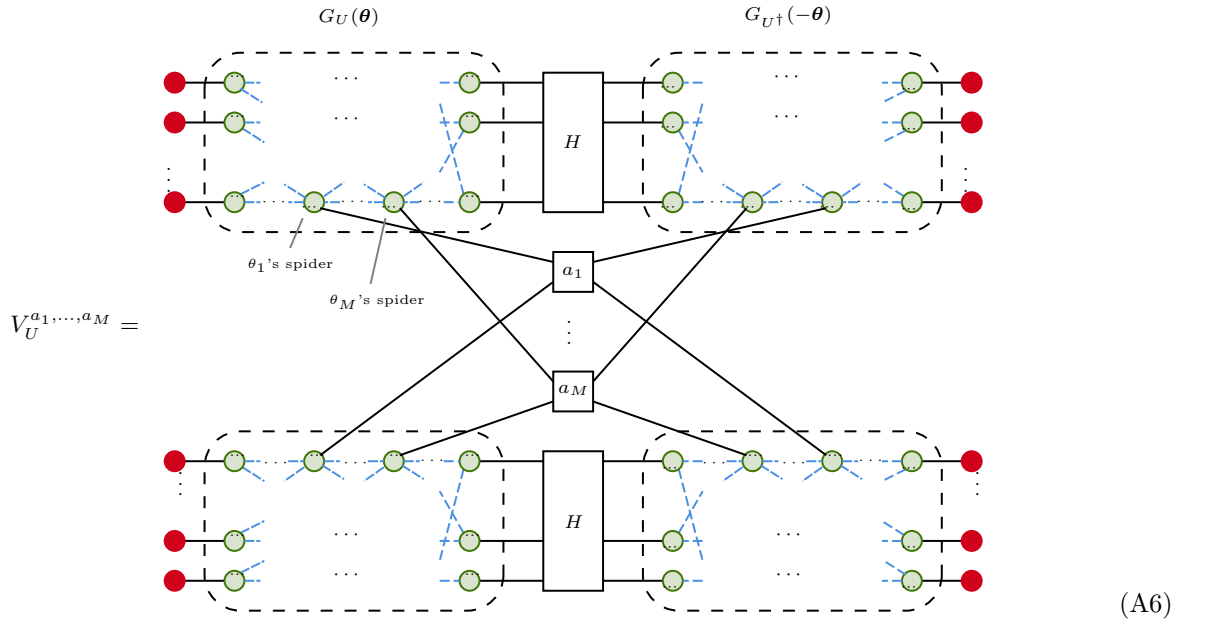
It is shown in [31] that the variance integral becomes

$$\text{Var} [\partial_j \langle H \rangle_{\theta}] = \frac{|c|^2}{4^n} \sum_{a_k \in \{T_1, T_2, T_3\}, k \neq j} V_U^{a_1, \dots, a_{j-1}, T_2, a_{j+1}, \dots, a_M} \quad (\text{A4})$$

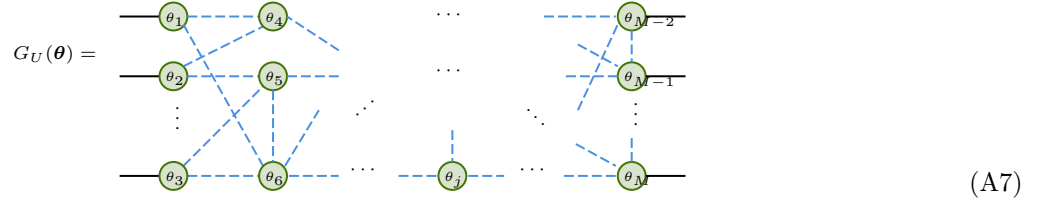
where



and for $a_i \in \{T_1, T_2, T_3\}$:

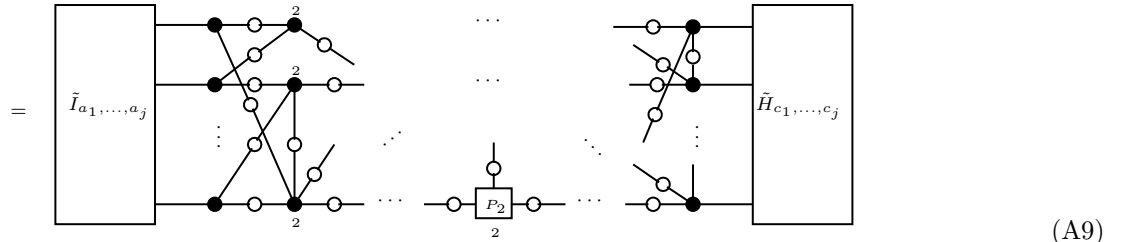


Analytically computing the sum of 3^{M-1} terms in Eq. (A4) is inefficient and does not clarify whether the parameterised circuit $U(\theta)$ suffers from barren plateaus. Thus the authors in [31] devise a way to simplify the expression (A4) directly from $G_U(\theta)$. Given a graph-like PQC



it is shown in [31] that

$$\text{Var} [\partial_j \langle H \rangle_{\theta}] = \frac{|c|^2}{4^n} \sum V_U^{a_1, \dots, a_k, b_1, \dots, b_l, \dots, T_2, \dots, c_1, \dots, c_M} \quad (\text{A8})$$



where the parameters $\theta_{k \neq j}$ in the graph-like PQC in (A7) are replaced by the copy tensor

$$in \left\{ \begin{array}{c} \diagup \diagdown \\ \bullet \\ \diagdown \diagup \end{array} \right\} out = \sum_{i=0}^2 |i\rangle^{\otimes \text{in}} \langle i|^{\otimes \text{out}}, \quad (\text{A10})$$

the parameter θ_j is replaced by the projection onto the second dimension

$$in \left\{ \begin{array}{c} \diagup \diagdown \\ \square \\ \diagdown \diagup \end{array} \right\} out = \sum_{i=0}^2 |i\rangle^{\otimes \text{in}} \langle 1|^{\otimes \text{out}} \quad (\text{A11})$$

and each Hadamard edge is replaced by the 3×3 matrix

$$\text{---o---} = \frac{1}{4} \begin{bmatrix} 1 & 1 & 1 \\ 1 & 1 & -1 \\ 1 & -1 & 1 \end{bmatrix} =: M. \quad (\text{A12})$$

The tensors $\tilde{I}_{a_1, \dots, a_j}$ and $\tilde{H}_{c_1, \dots, c_M}$ are related to the initial state and the observable H , respectively. In this article the initial state is $|0\rangle^{\otimes N}$ and so \tilde{I} is

$$N \left\{ \begin{array}{c} \frac{1}{4} \bullet^2 \\ \frac{1}{4} \bullet^2 \\ \vdots \\ \frac{1}{4} \bullet^2 \end{array} \right\} \quad (\text{A13})$$

If $H = \sigma_1 \otimes \dots \otimes \sigma_N$ where $\sigma_i = k_{i,0}I + k_{i,1}X + k_{i,2}Y + k_{i,3}Z$ is a sum of Pauli terms acting on qubit i , it is proven in [31] that $\tilde{H} = \mathbf{u}_1 \otimes \dots \otimes \mathbf{u}_N$, where

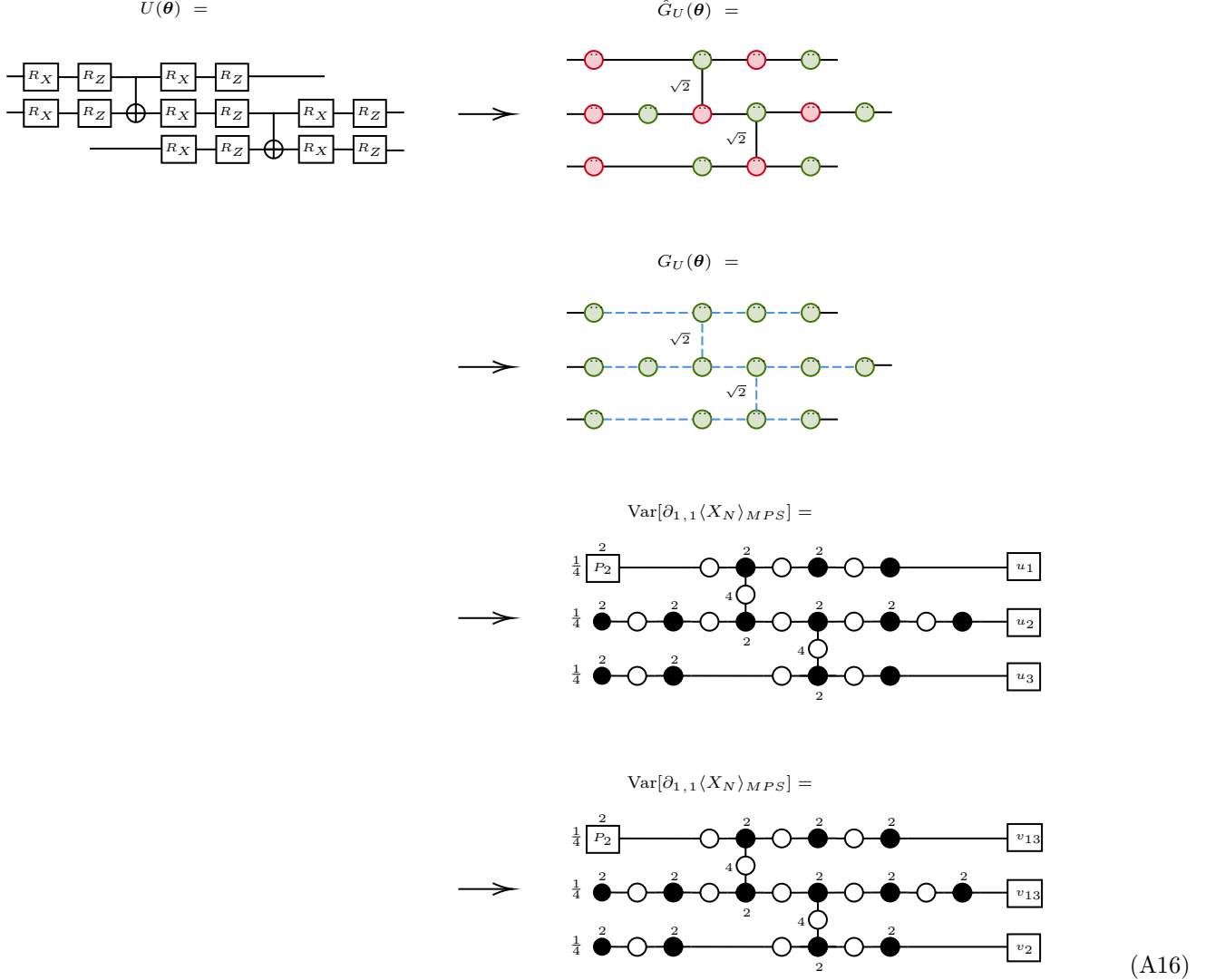
$$u_i = 2k_{i,0}^2 \mathbf{v}_{13} + 2(k_{i,1}^2 + k_{i,3}^2) \mathbf{v}_2 + 2k_{i,2}^2 \mathbf{v}_{13}^- \quad (\text{A14})$$

and

$$\mathbf{v}_{13} = \begin{bmatrix} 1 \\ 0 \\ 1 \end{bmatrix}, \quad \mathbf{v}_2 = \begin{bmatrix} 0 \\ 1 \\ 0 \end{bmatrix}, \quad \mathbf{v}_{13}^- = \begin{bmatrix} 1 \\ 0 \\ -1 \end{bmatrix}. \quad (\text{A15})$$

Continuing the example for the 3-qubit qMPS from the beginning of this Appendix, the variance of the gradient of

the first (top left) parameter for the observable $H = X_3$ can be found by evaluating



Appendix B: Quantum matrix product states

The qMPS ansatz of Eq. (9) for N qubits has the form

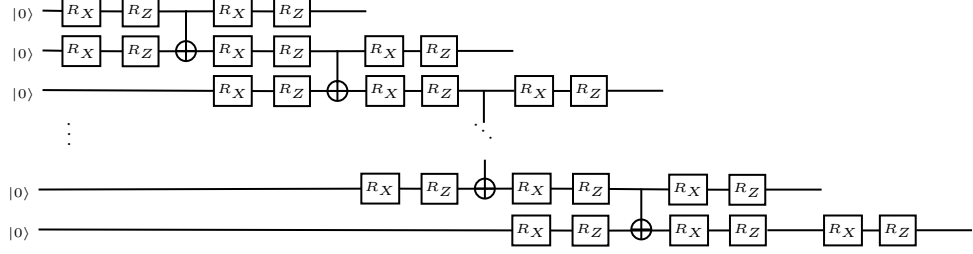
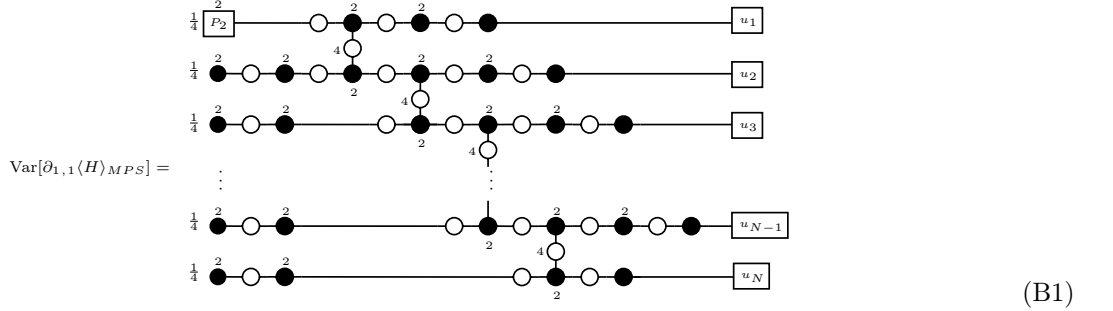


Figure 3: The qMPS circuit considered in this article.

We index parameters using the index pair (j, k) which refers to the k -th parameter in qubit register $j = 1, \dots, N$.

Theorem 2 and App. A imply that



where the gradient is calculated for the first parameter on the first qubit register and the vectors u_i are related to the observables via Eq. (A14). To consider general parameters (j, k) we simply move the projection P_2 to the copy tensor at position (j, k) . Using the identities

$$2M\mathbf{v}_{13} = \mathbf{v}_{13}, \quad 2M\mathbf{v}_2 = \frac{1}{2}(\mathbf{v}_2 + \mathbf{v}_{13}^-), \quad 2M\mathbf{v}_{13}^- = \mathbf{v}_2, \quad (B2)$$

and

$$\begin{aligned} \begin{array}{c} \text{---} \\ \text{---} \end{array} \begin{array}{c} \text{---} \\ \text{---} \end{array} \begin{array}{c} \text{---} \\ \text{---} \end{array} &= \frac{1}{2} \left\{ \begin{array}{c} \text{---} \\ \text{---} \end{array} \begin{array}{c} \text{---} \\ \text{---} \end{array} \right. , \quad \begin{array}{c} \text{---} \\ \text{---} \end{array} \begin{array}{c} \text{---} \\ \text{---} \end{array} \begin{array}{c} \text{---} \\ \text{---} \end{array} &= \left\{ \begin{array}{c} \text{---} \\ \text{---} \end{array} \begin{array}{c} \text{---} \\ \text{---} \end{array} \right. , \quad \begin{array}{c} \text{---} \\ \text{---} \end{array} \begin{array}{c} \text{---} \\ \text{---} \end{array} \begin{array}{c} \text{---} \\ \text{---} \end{array} &= \left\{ \begin{array}{c} \text{---} \\ \text{---} \end{array} \begin{array}{c} \text{---} \\ \text{---} \end{array} \right. \end{aligned} \quad (B3)$$

for M as in Eq. (A12) and $\mathbf{v}_{13}, \mathbf{v}_2, \mathbf{v}_{13}^-$ as in Eq. (A15) we show that the contributions of X_i, Y_i, Z_i to the variance are the same up to a constant factor:

Lemma 1. Let $\sigma_i = I^{\otimes i-1} \otimes \sigma \otimes I^{\otimes n-i}$ where $\sigma \in \{X, Y, Z\}$ is a Pauli matrix. Then

$$\text{Var}[\partial_{1,1} \langle X_i \rangle] = \text{Var}[\partial_{1,1} \langle Z_i \rangle] = c \text{Var}[\partial_{1,1} \langle Y_i \rangle] \quad (B4)$$

for some constant c .

Proof. For the first equality, note that by Eq. (A14) both observables X_i and Z_i yield $u_i = 2\mathbf{v}_2$ and $u_{i' \neq i} = 2\mathbf{v}_{13}$ so that the contraction in Eq. (B1) is the same in both cases. For the second equality, observable Y_i yields $u_i = 2\mathbf{v}_{13}^-$ and $u_{i' \neq i} = 2\mathbf{v}_{13}$ and Eqs. (B2), (B3) imply

$$\begin{aligned} \begin{array}{c} \text{---} \\ \text{---} \end{array} \begin{array}{c} \text{---} \\ \text{---} \end{array} \begin{array}{c} \text{---} \\ \text{---} \end{array} &= \left\{ \begin{array}{c} \text{---} \\ \text{---} \end{array} \begin{array}{c} \text{---} \\ \text{---} \end{array} \right. + \left\{ \begin{array}{c} \text{---} \\ \text{---} \end{array} \begin{array}{c} \text{---} \\ \text{---} \end{array} \right. + \frac{1}{2} \left\{ \begin{array}{c} \text{---} \\ \text{---} \end{array} \begin{array}{c} \text{---} \\ \text{---} \end{array} \right. \\ &= \left\{ \begin{array}{c} \text{---} \\ \text{---} \end{array} \begin{array}{c} \text{---} \\ \text{---} \end{array} \right. + \left\{ \begin{array}{c} \text{---} \\ \text{---} \end{array} \begin{array}{c} \text{---} \\ \text{---} \end{array} \right. + \frac{1}{2} \left\{ \begin{array}{c} \text{---} \\ \text{---} \end{array} \begin{array}{c} \text{---} \\ \text{---} \end{array} \right. \end{aligned} \quad (B5)$$

where the vector $c_{13}\mathbf{v}_{13} + c_2\mathbf{v}_2 + c_{13}^-\mathbf{v}_{13}^-$ for non-negative constants c_{13}, c_{13}^-, c_2 in the i -th register comes from contracting all registers $i' > i$ in the tensor network in (B1). In particular, note that the right-hand side above no longer carries a \mathbf{v}_{13}^- term on the $(i-1)$ -th register. Additionally the two terms on the right side leading with a \mathbf{v}_{13} on the top register do not contribute to the variance as they will eventually be discarded by the projection. Hence the tensor network is fully determined by the third term on the right-hand side and therefore equivalent to the one corresponding to the observables X_i and Z_i , up to the constant factor c_2 accrued from contracting the registers $i' > i$ ⁴. \square

This Lemma implies that it suffices to consider the 1-local observable X_i to probe the behaviour of the variance for general 1-local operators. Also, this Lemma trivially generalises to the qTTN and qMERA circuits and, therefore, henceforth we focus solely on observables X_i .

Theorem 7. *Let $\langle X_i \rangle_{qMPS}$ be the cost function associated with the observable X_i and consider the qMPS ansatz for N qubits defined in Eq. (9), then:*

$$\text{Var}[\partial_{1,1}\langle X_i \rangle_{qMPS}] = \begin{cases} \frac{1}{4} \cdot \left(\frac{3}{8}\right)^{N-1} & \text{if } i = N, \\ 11 \cdot \left(\frac{1}{8}\right)^2 \cdot \left(\frac{3}{8}\right)^{i-1} & \text{if } 1 < i < N, \\ \frac{11}{8^2} & \text{if } i = 1, \end{cases} \quad (\text{B6})$$

where $\partial_{1,1}\langle X_i \rangle_{qMPS}$ refers to the gradient w.r.t. the 1-st parameter in the 1-st qubit register.

Proof. $\text{Var}[\partial_{1,1}\langle X_i \rangle]$ can be found for the three separate cases by contracting the tensor network in Eq. (B1) with $u_i = \mathbf{v}_2$ and $u_{i' \neq i} = \mathbf{v}_{13}$. Given Eqs. (B2), (B3) this is a straightforward calculation from which we also derive the useful identity

$$\begin{array}{c} \text{Diagram showing a tensor network with a central node labeled } \{c_{13}\mathbf{v}_{13} + c_2\mathbf{v}_2 + c_{13}^-\mathbf{v}_{13}^-\} \text{ connected to two terms: } -\mathbf{v}_{13} \text{ and } -\mathbf{v}_2. \end{array} = \begin{cases} -\mathbf{v}_{13} \\ c_{13} + \frac{c_{13}^-}{4} \end{cases} + \begin{cases} -\mathbf{v}_2 \\ \frac{3c_2}{8} \end{cases} \quad (\text{B7})$$

which repeats on every register in Eq. (B1), for non-negative constants c_{13}, c_{13}^-, c_2 . \square

Computing the gradient variance for a general parameter indexed by (j, k) can be done analogously by moving the projection P_2 in Eq. (B1) to the copy tensor at position (j, k) . The calculation can be simplified by, first, identifying the cases in which the triple index (i, j, k) gives $\text{Var}[\partial_{j,k}\langle X_i \rangle_{qMPS}] = 0$. Figure 4 illustrates the causal cone corresponding to observable X_i in a qMPS circuit. We observe that in the qMPS the triple index (i, j, k) for which $\text{Var}[\partial_{j,k}\langle X_i \rangle_{qMPS}] = 0$ satisfies

$$\text{Var}[\partial_{j,k}\langle X_i \rangle_{qMPS}] = 0 \quad \text{if} \quad \begin{cases} j > i + 1 \ \forall k, \\ j = i + 1 \text{ and } k > 2, \\ j < i \text{ and } k > 4 \ (k > 2 \text{ for } j = 1). \end{cases} \quad (\text{B8})$$

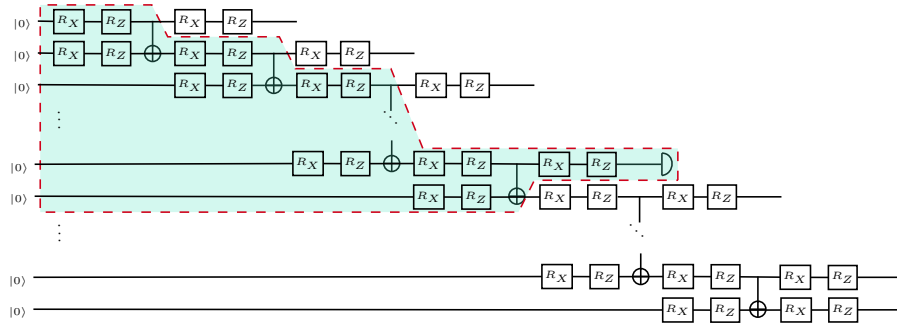


Figure 4: Causal cone for a 1-local observable.

The definition for the causal cone of a PQC can be extended analogously to apply to the variance tensor networks of the form of Eq. (A8) —for example Eq. (B1).

⁴ In fact the registers $i' > i$ which have a \mathbf{v}_{13} at the end and are not directly (nearest-neighbour) connected to a \mathbf{v}_2 or \mathbf{v}_{13}^- contract to the identity.

Theorem 8. Let $\langle X_i \rangle_{qMPS}$ be the cost function associated with the observable X_i and consider the qMPS ansatz defined in Eq. (9), then:

$$\text{Var}[\partial_{j,1} \langle X_N \rangle_{qMPS}] = \begin{cases} \frac{1}{4} \cdot \left(\frac{3}{8}\right)^{N-1} & \text{if } j < N, \\ \frac{1}{4} \left(1 + \left(\frac{3}{8}\right)^{N-1}\right) & \text{if } j = N, \end{cases} \quad (\text{B9})$$

$$\text{Var}[\partial_{j,1} \langle X_i \rangle_{qMPS}] = \begin{cases} 11 \cdot \left(\frac{1}{8}\right)^2 \left(\frac{3}{8}\right)^{i-1} & \text{if } j < i, \\ 3 \cdot \left(\frac{1}{8}\right)^2 \left(1 + \frac{11}{8} \cdot \left(\frac{3}{8}\right)^{i-2}\right) & \text{if } j = i, \\ 3 \cdot \left(\frac{1}{8}\right)^2 \left(1 + \left(\frac{3}{8}\right)^{i-1}\right) & \text{if } j = i+1, \end{cases} \quad (\text{B10})$$

where $\partial_{j,1} \langle X_i \rangle_{qMPS}$ refers to the gradient w.r.t. the 1-st parameter in the j -th qubit register.

Proof. This is a straightforward contraction of the tensor network in Eq. (B1) but with the projection P_2 replacing the copy tensor indexed by (j, k) and using Eqs. (B2), (B3), (B7). \square

Remark 1. It is clear from this Theorem that $\text{Var}[\partial_{j,1} \langle X_i \rangle_{qMPS}] \geq \text{Var}[\partial_{1,1} \langle X_i \rangle_{qMPS}]$ for all $i = 1, \dots, N$ and all $j = 1, \dots, i+1$ but, in fact, this result also generalises to all (j, k) for which $\text{Var}[\partial_{j,k} \langle X_i \rangle_{qMPS}] \neq 0$. Indeed, each step in the contraction of the tensor network in Eq. (B1) increases the coefficients of the vectors $\mathbf{v}_{13}, \mathbf{v}_2$ and \mathbf{v}_{13}^- monotonically and, therefore, the earlier the projection P_2 is placed, the larger these coefficients become after the contributions of \mathbf{v}_{13} and \mathbf{v}_{13}^- are removed by P_2 . This argument applies analogously to qTTN and qMERA.

Now we consider k -local operators of the form $X_I := X_{i_1} \otimes \dots \otimes X_{i_k}$ for $I = \{i_1, \dots, i_k\}$ (w.l.o.g. $i_1 < i_2 < \dots < i_k$) and use techniques and results from this Appendix to justify Conjecture 1. The proof of Theorem 7 and the causal cone structure in Fig. 4 suggest that $\text{Var}[\partial_{1,1} \langle X_I \rangle_{qMPS}]$ vanishes exponentially with i_k . Our intuition is that barren plateaus appear when the causal cone of an observable includes a large number of qubits ($\approx N$) and we know that the causal cone relating to X_I contains at most $i_k + 1$ qubits for the qMPS ansatz in Fig. 3.

Theorem 9. Let $\langle X_i X_{i+1} \rangle_{qMPS}$ be the cost function associated with the observable $X_i X_{i+1}$ and consider the qMPS ansatz of Eq. (9), then:

$$\text{Var}[\partial_{1,1} \langle X_i X_{i-1} \rangle_{qMPS}] = c_i \left(\frac{3}{8}\right)^i, \quad (\text{B11})$$

where

$$c_i = \begin{cases} \frac{1}{4} \cdot \left(\left(\frac{3}{8}\right)^2 + \frac{13}{16}\right) & \text{if } i = 1, \\ \frac{1}{4} \cdot \left(\frac{37}{2 \cdot 8^2} + \frac{3}{16}\right) & \text{if } 1 < i < N, \\ \frac{37}{3 \cdot 8^2} & \text{if } i = N-1, \end{cases} \quad (\text{B12})$$

where $\partial_{1,1} \langle X_i \rangle_{qMPS}$ refers to the gradient w.r.t. the 1-st parameter in the 1-st qubit register.

Proof. $\text{Var}[\partial_{1,1} \langle X_i X_{i+1} \rangle_{qMPS}]$ can be found for the three separate cases by contracting the tensor network in Eq. (B1) with $\mathbf{u}_i = \mathbf{u}_{i+1} = \mathbf{v}_2$ and $u_{i' \neq i, i+1} = \mathbf{v}_{13}$ using Eqs. (B2), (B3), (B7) in addition to:

$$\begin{array}{c} \text{Diagram: } \begin{array}{c} \text{Two circles (1, 2) connected to a box } v_2. \text{ Below them, two circles (4, 2) connected to a box } v_2. \text{ Below them, two circles (2, 2) connected to a box } v_2. \end{array} \\ = \frac{1}{4} \left\{ \begin{array}{l} -v_2 + -v_{13}^- \\ -v_2 + v_{13}^- \end{array} \right\}, \end{array} \quad \begin{array}{c} \text{Diagram: } \begin{array}{c} \text{Two circles (1, 2) connected to a box } v_{13}^- \text{ (top). Below them, two circles (4, 2) connected to a box } v_2. \text{ Below them, two circles (2, 2) connected to a box } v_2. \end{array} \\ = \frac{1}{2} \left\{ \begin{array}{l} -v_2 \\ -v_2 + -v_{13}^- \end{array} \right\}, \end{array} \quad \begin{array}{c} \text{Diagram: } \begin{array}{c} \text{Two circles (1, 2) connected to a box } v_{13} \text{ (top). Below them, two circles (4, 2) connected to a box } v_{13}^- \text{ (bottom). Below them, two circles (2, 2) connected to a box } v_2. \end{array} \\ = \left\{ \begin{array}{l} -v_2 \\ -v_2 \end{array} \right\} \end{array} \quad (\text{B13})$$

\square

With the techniques from this Appendix, we are ready to discuss the following proposition:

Conjecture 4. Provided $k \ll N$ the k -local operators of the form X_I acting on qubits $I = \{i_1, \dots, i_k\}$ with $i_1 < \dots < i_k$ satisfy $\text{Var}[\partial_{1,1} \langle X_I \rangle_{qMPS}] \in \Omega(c^{-i_k})$ for some $c > 1$.

The cases $k = 1, 2$ are covered in Theorem 3 and Theorem 4. For $k > 2$ we argue as follows: Given a k -local operator acting on qubits $I = \{i_1, \dots, i_k\}$ with $i_1 < \dots < i_k$, then $\text{Var}[\partial_{1,1} \langle X_I \rangle_{qMPS}]$ corresponds to a tensor network as in Eq. (B1) but where all registers below the $(i_k + 1)$ -th qubit do not contribute to the variance. Hence when contracting the network we accrue contributions from at most $(i_k + 1)$ registers.

Appendix C: Quantum tree tensor networks

For $N = 2^n$ qubits the qTTN ansatz of Eq. (17) is

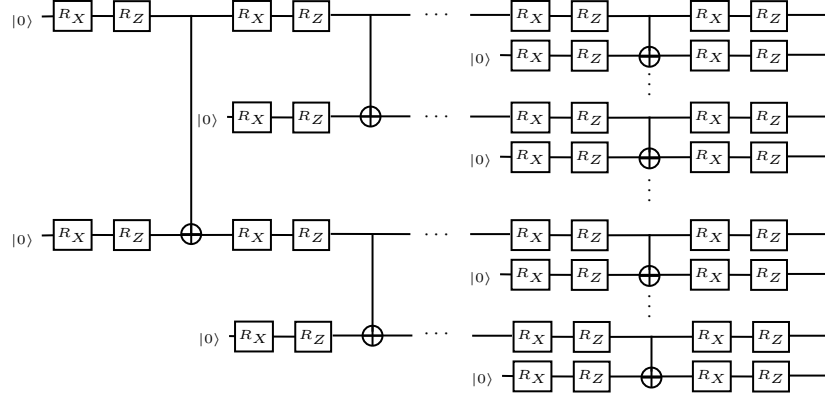
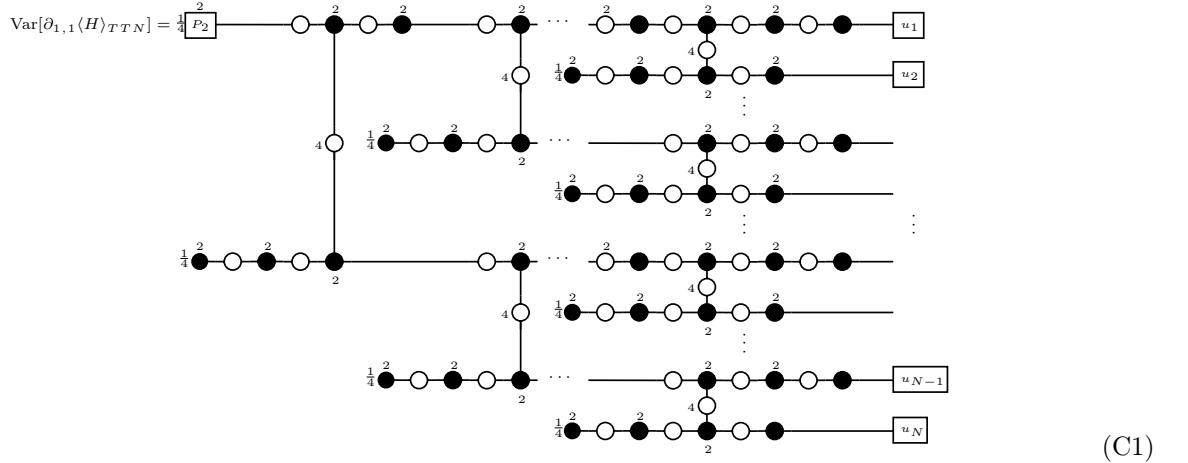


Figure 5: qTTN circuit considered in this article.

Theorem 2 and Appendix A imply that

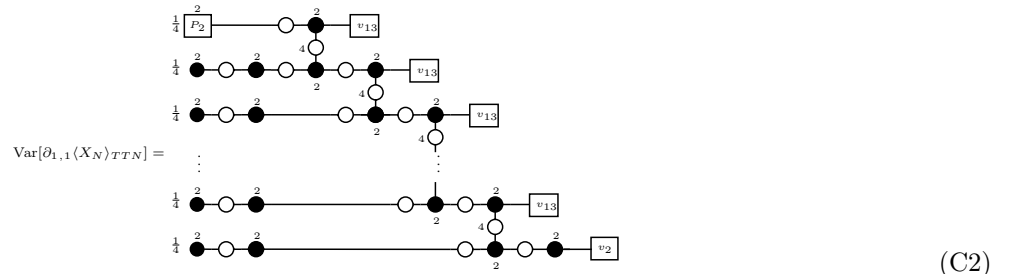


In particular note that the causal cone of any observable in the circuit of Fig. 5 —equivalently, any vector u_i in Eq. (C1)— contains exactly $1 + \log(N) = 1 + n$ registers. We deduce:

Theorem 10. *Let $\langle X_i \rangle_{qTTN}$ be the cost function associated with the observable X_i and consider the qTTN ansatz defined in Eq. (17), then:*

1. $\text{Var}[\partial_{1,1} \langle X_N \rangle_{qTTN}] = \frac{1}{4} \cdot \left(\frac{3}{8}\right)^n,$
2. $\text{Var}[\partial_{1,1} \langle X_1 \rangle_{qTTN}] \in \Omega\left(\left(\frac{\lambda_2}{4}\right)^n\right)$ where $\lambda_2 \approx 2.3187$.

Proof. We consider $\text{Var}[\partial_{1,1} \langle X_N \rangle_{qTTN}]$ first: The parameters not causally connected to X_N in Eq. (C1) contract to the identity, reducing the variance to:



where there are a total of $1 + n$ registers. The contraction here is identical to the one in the proof of Theorem 7 but with an extra register, which gives $\text{Var}[\partial_{1,1}\langle X_N \rangle_{\text{qTTN}}] = \frac{1}{4} \cdot \left(\frac{3}{8}\right)^n$. For the second statement, contracting all the registers not causally connected to X_1 yields

$$\begin{aligned}
\text{Var}[\partial_{1,1} \langle X_1 \rangle_{TTN}] &= \frac{1}{4} \boxed{P_2} \xrightarrow{\quad} \text{Diagram 1} \quad \left[\text{Diagram 2} \right] \quad \times (n-1) \\
&= \frac{1}{4} \boxed{P_2} \xrightarrow{\quad} \text{Diagram 1} \quad \left[\text{Diagram 2} \right] \quad \times (n-1) \\
&= \frac{1}{4} \boxed{P_2} \xrightarrow{\quad} \text{Diagram 1} \quad \left[\text{Diagram 2} \right] \quad \boxed{\frac{3}{4}v_2 + \frac{1}{4}v_{13}} \quad (C3)
\end{aligned}$$

which we simplify by noting that

$$\begin{array}{c} \text{Diagram 1: } \text{A directed graph with 6 nodes. The top row has nodes } 2, 2, \text{ and } v_2 \text{ (square). The bottom row has nodes } 2, 2, 4, \text{ and } v_{13} \text{ (square). Directed edges: } 2 \rightarrow 2, 2 \rightarrow v_2, 2 \rightarrow 2, 2 \rightarrow 2, 2 \rightarrow 4, 2 \rightarrow v_{13}, 2 \rightarrow 2, 2 \rightarrow 2, 2 \rightarrow 4, 2 \rightarrow v_{13}, 2 \rightarrow 2. \text{ Total weight: } 2+2+4+2+2+2+2+2+2+2+2+2 = 24. \\ \text{Diagram 2: } \text{A directed graph with 6 nodes. The top row has nodes } 2, 2, \text{ and } v_{13}^- \text{ (square). The bottom row has nodes } 2, 2, 4, \text{ and } v_{13} \text{ (square). Directed edges: } 2 \rightarrow 2, 2 \rightarrow v_{13}^-, 2 \rightarrow 2, 2 \rightarrow 2, 2 \rightarrow 4, 2 \rightarrow v_{13}, 2 \rightarrow 2, 2 \rightarrow 2, 2 \rightarrow 4, 2 \rightarrow v_{13}, 2 \rightarrow 2. \text{ Total weight: } 2+2+4+2+2+2+2+2+2+2+2+2 = 24. \end{array} = \frac{1}{4}(3\mathbf{v}_2 + \mathbf{v}_{13}^-), \quad 2(\mathbf{v}_2 + \mathbf{v}_{13}^-). \quad (\text{C4})$$

If we denote the resulting vector after the k -th application of the term within the square brackets in Eq. (C3) by $\mathbf{v}_k = \frac{1}{4}(\alpha_k \mathbf{v}_2 + \beta_k \mathbf{v}_{13}^-)$ with $\mathbf{v}_0 = \frac{1}{4}(3\mathbf{v}_2 + \mathbf{v}_{13}^-)$, then by using the identities in Eq. (C4) we find that any subsequent term is given by $\mathbf{v}_{k+1} = \frac{1}{4}(\alpha_{k+1} \mathbf{v}_2 + \beta_{k+1} \mathbf{v}_{13}^-)$ for

$$\alpha_{k+1} = \frac{1}{4}(3\alpha_k + 8\beta_k) \quad \text{and} \quad \beta_{k+1} = \frac{1}{4}(\alpha_k + 8\beta_k). \quad (\text{C5})$$

Let $\mathbf{u}_k := \frac{1}{4}[\alpha_k, \beta_k]^T$ be the coefficient vector associated with \mathbf{v}_k , then the transformation $\mathbf{v}_k \rightarrow \mathbf{v}_{k+1}$ is determined by the linear map:

$$M : \mathbf{u}_k \mapsto \mathbf{u}_{k+1}, \quad M = \frac{1}{4} \begin{bmatrix} 3 & 8 \\ 1 & 8 \end{bmatrix}. \quad (\text{C6})$$

M has eigenvalues $\lambda_1 \approx 0.4313$ and $\lambda_2 \approx 2.3187$ and respective eigenvectors $\mathbf{w}_1, \mathbf{w}_2$ so that the spectral theorem implies that after the application of the $(n - 1)$ terms in the square brackets we obtain

$$\mathbf{u}_{n-1} = \begin{bmatrix} \alpha_{n-1} \\ \beta_{n-1} \end{bmatrix} = M^{n-1} \mathbf{u}_0 = [\mathbf{w}_1, \mathbf{w}_2] \begin{bmatrix} \lambda_1^{n-1} & 0 \\ 0 & \lambda_2^{n-1} \end{bmatrix} [\mathbf{w}_1, \mathbf{w}_2]^{-1} \mathbf{u}_0. \quad (C7)$$

Contracting the rest of the tensor network then gives

$$\begin{aligned}
& \text{Var}[\partial_{1,1} \langle X_1 \rangle_{TTN}] = \\
& \quad \text{Diagram 1: } \frac{1}{4^{n+1}} \text{ } P_2 \text{ } \xrightarrow{2} \text{ } \text{Diagram 2: } \frac{2}{4^{n+1}} \text{ } P_2 \text{ } \xrightarrow{2} \text{ } \text{Diagram 3: } \frac{2}{4^{n+1}} \text{ } P_2 \text{ } \xrightarrow{2} \text{ } \text{Diagram 4: } \frac{2}{4^{n+1}} \text{ } P_2 \text{ } \xrightarrow{2} \text{ } \text{Diagram 5: } \frac{2}{4^{n+1}} \text{ } P_2 \text{ } \xrightarrow{2} \\
& \quad \text{Diagram 1: } \frac{1}{4^{n+1}} \text{ } P_2 \text{ } \xrightarrow{2} \text{ } \text{Diagram 2: } \frac{2}{4^{n+1}} \text{ } P_2 \text{ } \xrightarrow{2} \text{ } \text{Diagram 3: } \frac{2}{4^{n+1}} \text{ } P_2 \text{ } \xrightarrow{2} \text{ } \text{Diagram 4: } \frac{2}{4^{n+1}} \text{ } P_2 \text{ } \xrightarrow{2} \text{ } \text{Diagram 5: } \frac{2}{4^{n+1}} \text{ } P_2 \text{ } \xrightarrow{2} \\
& = \frac{1}{4^{n+1}} \text{ } P_2 \text{ } \xrightarrow{2} + \frac{\alpha_{n-1}}{2} \left\{ \begin{array}{l} \text{Diagram 3: } \frac{2}{4^{n+1}} \text{ } P_2 \text{ } \xrightarrow{2} \text{ } \text{Diagram 4: } \frac{2}{4^{n+1}} \text{ } P_2 \text{ } \xrightarrow{2} \text{ } \text{Diagram 5: } \frac{2}{4^{n+1}} \text{ } P_2 \text{ } \xrightarrow{2} \\ \text{Diagram 3: } \frac{2}{4^{n+1}} \text{ } P_2 \text{ } \xrightarrow{2} \text{ } \text{Diagram 4: } \frac{2}{4^{n+1}} \text{ } P_2 \text{ } \xrightarrow{2} \text{ } \text{Diagram 5: } \frac{2}{4^{n+1}} \text{ } P_2 \text{ } \xrightarrow{2} \end{array} \right\} + \beta_{n-1} \left\{ \begin{array}{l} \text{Diagram 3: } \frac{2}{4^{n+1}} \text{ } P_2 \text{ } \xrightarrow{2} \text{ } \text{Diagram 4: } \frac{2}{4^{n+1}} \text{ } P_2 \text{ } \xrightarrow{2} \text{ } \text{Diagram 5: } \frac{2}{4^{n+1}} \text{ } P_2 \text{ } \xrightarrow{2} \\ \text{Diagram 3: } \frac{2}{4^{n+1}} \text{ } P_2 \text{ } \xrightarrow{2} \text{ } \text{Diagram 4: } \frac{2}{4^{n+1}} \text{ } P_2 \text{ } \xrightarrow{2} \text{ } \text{Diagram 5: } \frac{2}{4^{n+1}} \text{ } P_2 \text{ } \xrightarrow{2} \end{array} \right\} \\
& = \frac{1}{4^{n+1}} (\alpha_{n-1} + 8\beta_{n-1}). \tag{C9}
\end{aligned}$$

We approximate the above by noticing that for n large enough, $\lambda_2^{n-1} \gg \lambda_1^{n-1} \approx 0$ and so $\alpha_n, \beta_n \in O(\lambda_2^{n-1})$ so that

$$\text{Var} [\partial_{1,1} \langle X_1 \rangle_{\text{qTTN}}] = \frac{1}{4^{n+1}} (\alpha_{n-1} + 8\beta_{n-1}) \in \Omega\left(\left(\frac{\lambda_2}{4}\right)^n\right). \quad (\text{C10})$$

In general we obtain the gradient variance corresponding to any observable of the form X_i analytically by contracting the tensor network in Eq. (C1) using the identities in Eqs. (B2)–(B3)–(B7) as was demonstrated in the proof of

Theorem 10. When performing this contraction, we encounter two types of operations:

$$\begin{array}{c} \text{Diagram showing a contraction of a tensor network. The left side shows a sequence of tensors with indices 2, 4, 2, 4, 2. The right side shows the result of the contraction with indices 2, 4, 2, 4, 2. The result is a sum of three terms: } \\ \{c_{13}v_{13} + c_2v_2 + c_{13}^-v_{13}^-\} \end{array} = \begin{cases} -v_{13} \\ c_{13} + \frac{c_{13}^-}{4} \end{cases} + \begin{cases} -v_2 \\ \frac{3c_2}{8} \end{cases} \quad (\text{C11})$$

which occurs when the contribution to the variance originating from the observable travels ‘upwards’ in the tensor network in Eq. (C1) and

$$\begin{array}{c} \text{Diagram showing a contraction of a tensor network. The left side shows a sequence of tensors with indices 2, 4, 2, 4, 2. The right side shows the result of the contraction with indices 2, 4, 2, 4, 2. The result is a sum of three terms: } \\ \{c_{13}v_{13} + c_2v_2 + c_{13}^-v_{13}^-\} \end{array} = \begin{cases} -v_{13} \\ c_{13} \end{cases} + \begin{cases} -v_2 \\ \frac{c_2}{8} + c_{13} \end{cases} + \begin{cases} -v_{13}^- \\ \frac{c_2}{8} \end{cases} \quad (\text{C12})$$

which occurs when the contributions travels ‘downwards’ in the network in (C1). We refer to these as ‘up’ and ‘down’ operations, respectively. The constants $c_{13}, c_2, c_{13}^- \geq 0$. Indeed, for arbitrary i the tensor network contraction corresponding to $\text{Var}[\partial_{1,1}\langle X_i \rangle_{\text{qTTN}}]$ contains a mixture of the ‘up’ operations (C11) and the ‘down’ operations (C12). In the limit where all operations are ‘up’ (‘down’) we obtain $\text{Var}[\partial_{1,1}\langle X_N \rangle_{\text{qTTN}}]$ as in Eq. (C2) ($\text{Var}[\partial_{1,1}\langle X_1 \rangle_{\text{qTTN}}]$ as in Eq. (C3)). We emphasize that $\text{Var}[\partial_{1,1}\langle X_i \rangle_{\text{qTTN}}] \in \Theta(c^{-\log N})$ for arbitrary i , since the observable X_i is causally connected to $1 + \log N$ qubits and as such, when contracting the resulting tensor network in Eq. (C1), it can only pick up contributions from that many registers.

We show this explicitly in the following Lemma where we prove that $\text{Var}[\partial_{1,1}\langle X_N \rangle_{\text{qTTN}}]$ is a lower-bound to $\text{Var}[\partial_{1,1}\langle X_i \rangle_{\text{qTTN}}]$ for general i . Hence it is not necessary to compute $\text{Var}[\partial_{1,1}\langle X_i \rangle_{\text{qTTN}}]$ for all i to conclude that the qTTN ansatz does not have exponentially vanishing gradients. Together with Theorem 10 this implies that our qTTN ansatz completely avoids barren plateaus as the gradients only vanish polynomially in N , as claimed in Theorem 5 in the main text.

Lemma 2. *Let $\langle X_i \rangle_{\text{qTTN}}$ be the cost function associated with the observable X_i and consider the qTTN ansatz defined in Eq. (17), then:*

$$\text{Var}[\partial_{1,1}\langle X_N \rangle_{\text{qTTN}}] \leq \text{Var}[\partial_{1,1}\langle X_i \rangle_{\text{qTTN}}] \leq \text{Var}[\partial_{1,1}\langle X_1 \rangle_{\text{qTTN}}] \quad (\text{C13})$$

for all $i = 1, \dots, N$.

Proof. After identifying the $1 + \log N$ qubits causally connected with the observable X_i , the variance in Eq. (C1) reduces to a tensor network containing a mixture of ‘up’ operations (C11) and ‘down’ operations (C12). The transformation of the coefficients c_{13}, c_2, c_{13}^- is determined by

$$M_{\text{Up}} : \begin{bmatrix} c_{13} \\ c_2 \\ c_{13}^- \end{bmatrix} \mapsto \begin{bmatrix} c_{13} + c_{13}^-/4 \\ 3c_2/8 \\ 0 \end{bmatrix} \Rightarrow M_{\text{Up}} = \begin{bmatrix} 1 & 0 & 1/4 \\ 0 & 3/8 & 0 \\ 0 & 0 & 0 \end{bmatrix}, \quad (\text{C14})$$

$$M_{\text{Down}} : \begin{bmatrix} c_{13} \\ c_2 \\ c_{13}^- \end{bmatrix} \mapsto \begin{bmatrix} c_{13} \\ c_2/8 + c_{13}^- \\ c_2/8 \end{bmatrix} \Rightarrow M_{\text{Down}} = \begin{bmatrix} 1 & 0 & 0 \\ 0 & 1/8 & 1 \\ 0 & 1/8 & 0 \end{bmatrix}. \quad (\text{C15})$$

It suffices to show that the ‘up’ operation (C11) leads to a smaller contribution to the variance than the ‘down’ operation (C12). This is true because to find $\text{Var}[\partial_{1,1}\langle X_N \rangle_{\text{qTTN}}]$ by contraction of the tensor network in Eq. (C2) we need to perform operation (C11) n times, whereas to find $\text{Var}[\partial_{1,1}\langle X_i \rangle_{\text{qTTN}}]$ for general i by contraction of the tensor network in Eq. (C1) we need to perform a mixture of n ‘up’ and ‘down’ operations. Note that we are ultimately interested in the size of the coefficient c_2 as the other two coefficients will be disregarded by the P_2 at the top left parameter. If prior to the ‘down’ operation (C12) we have an arbitrary vector $c_{13}\mathbf{v}_{13} + c_2\mathbf{v}_2 + c_{13}^-\mathbf{v}_{13}^-$, then looking at Eqs. (C14), (C15) we find that $M_{\text{Up}} : c_2 \mapsto \frac{3c_2}{8}$ and $M_{\text{Down}} : c_2 \mapsto \frac{c_2}{8} + c_{13}^-$ and so we want to prove:

$$\frac{3c_2}{8} \leq \frac{c_2}{8} + c_{13}^- \quad \text{or equivalently} \quad c_2 \leq 4c_{13}^-. \quad (\text{C16})$$

Referencing the diagram in Eq. (C1) we show that this is always satisfied: Notice that a ‘down’ operation is always preceded by a $\text{---} \bullet$ on the top wire, i.e.

$$\begin{array}{c} \text{Diagram showing a contraction of a tensor network. The left side shows a sequence of tensors with indices 2, 4, 2, 4, 2. The right side shows the result of the contraction with indices 2, 4, 2, 4, 2. The result is a sum of three terms: } \\ \{c'_{13}v'_{13} + c'_2v'_2 + c'_{13}^-v'_{13}^-\} \end{array} = \begin{array}{c} \text{Diagram showing a contraction of a tensor network. The left side shows a sequence of tensors with indices 2, 4, 2, 4, 2. The right side shows the result of the contraction with indices 2, 4, 2, 4, 2. The result is a sum of three terms: } \\ \{c'_{13}v'_{13} + c'_2v'_2 + c'_{13}^-v'_{13}^-\} \end{array} \quad (\text{C17})$$

for some constants $c'_{13}, c'_2, c_{13}^{-\prime}$. Contracting the $\text{---} \bullet$ on the right hand side gives

$$\text{---} \bullet \{ \boxed{c'_{13} v_{13}} + \boxed{c'_2 v_2} + \boxed{c_{13}^{-\prime} v_{13}^-} \} = c'_{13} \mathbf{v}_{13} + \left(\frac{c'_2}{2} + c_{13}^{-\prime} \right) \mathbf{v}_2 + \frac{c'_2}{2} \mathbf{v}_{13}^-, \quad (\text{C18})$$

which reduces requirement (C16) to

$$\left(\frac{c'_2}{2} + c_{13}^{-\prime} \right) \leq 4 \cdot \left(\frac{c'_2}{2} \right) \quad \text{or equivalently} \quad 2c_{13}^{-\prime} \leq 3c'_2. \quad (\text{C19})$$

To analyse these we check the operation preceding the right hand side of Eq. (C17) leading to the constants $c'_{13}, c'_2, c_{13}^{-\prime}$, which is either the ‘up’ operation (C11), the ‘down’ operation (C12) or the observable u_i itself:

- If ‘up’, then Eq. (C14) implies $c_{13}^{-\prime} = 0$ which trivially satisfies requirement (C19).
- If ‘down’, then we consider the vector $c''_{13} \mathbf{v}_{13} + c''_2 \mathbf{v}_2 + c_{13}''^- \mathbf{v}_{13}^-$ which precedes it:

$$c'_{13} \mathbf{v}_{13} + c'_2 \mathbf{v}_2 + c_{13}^{-\prime} \mathbf{v}_{13}^- = \text{---} \bullet \{ \boxed{c''_{13} v_{13}} + \boxed{c''_2 v_2} + \boxed{c_{13}''^- v_{13}^-} \} \quad (\text{C20})$$

Equation (C15) implies:

$$c'_{13} = c''_{13}, \quad c'_2 = \frac{c''_2}{8} + c_{13}''^-, \quad c_{13}^{-\prime} = \frac{c''_2}{8}, \quad (\text{C21})$$

in which case $2c_{13}^{-\prime} = \frac{2c''_2}{8}$ and $3c'_2 = \frac{3c''_2}{8} + 3c_{13}''^-$, so that requirement (C19) is satisfied.

- Lastly, if the original ‘down’ is connected to the observable, we have

$$\text{---} \bullet \{ \boxed{c'_{13} v_{13}} + \boxed{c'_2 v_2} + \boxed{c_{13}''^- v_{13}^-} \} = \text{---} \bullet \{ \boxed{c'_{13} v_{13}} + \boxed{c'_2 v_2} + \boxed{c_{13}''^- v_{13}^-} \} \quad (\text{C22})$$

The identities in (B2) imply that $c_{13}^{-\prime} = c'_2 = \frac{1}{2}$ and so requirement (C19) is satisfied.

This concludes the proof. \square

Note that the inequality in the Lemma is just a consequence of the order of the qubits in the construction of the ansatz in Fig. 5. We expect that the variance of any pair of observables X_{i_1}, X_{i_2} in the qTTN ansatz vanishes identically modulo a different base, i.e. $\text{Var}[\partial_{1,1} \langle X_i \rangle_{\text{qTTN}}]$ vanishes as $c_i^{\log N}$ for each i and some $c_i > 0$. Indeed, we could achieve any other register ordering through SWAP gates without affecting the overall trainability of the ansatz.

Using the tools of the proof of Lemma 2 we now discuss Conjecture 2. We have established that observable X_i is causally connected to $(1 + \log N)$ qubits and so it follows that a k -local observable X_I acting on qubits $I = \{i_1, \dots, i_k\}$ is causally connected to at most $k(1 + \log N)$ qubits. This bound is usually not tight since there can be some overlap between the qubits causally connected to pairs $X_{i_{j_1}}, X_{i_{j_2}}$ for $i_{j_1}, i_{j_2} \in I$. Since Lemma 2 implies that contributions to the variance $\text{Var}[\partial_{1,1} \langle X_i \rangle]$ are smallest when the observable is X_N (i.e. when Eq. (C1) contracts to only ‘up’ operations (C11)), we argue that

$$\text{Var}[\partial_{1,1} \langle X_I \rangle_{\text{qTTN}}] \geq \text{Var}[\partial_{1,1} \langle X_{\hat{N}} \rangle_{\text{qTTN}}] = \frac{1}{4} \cdot \left(\frac{3}{8} \right)^{k \log N}, \quad (\text{C23})$$

where $\hat{N} = 2^{k \log N}$. Rather than having ‘up’ and ‘down’ operations from X_{i_j} for each $i_j \in I$ (cf. Eq. (C1) but with \mathbf{v}_2 in registers $I = \{i_1, \dots, i_k\}$ and \mathbf{v}_{13} elsewhere), the contributions to the variance are smallest when contracting a network as in Eq. (C2) that has $k \log N$ registers instead where there are only ‘up’ operations from the observable $X_{\hat{N}}$. Note that in the regime $k \approx N$ the number of qubits causally connected to X_I is N and we obtain exponentially vanishing gradients.

Appendix D: Quantum multiscale entanglement renormalization ansatz

For $8 = 2^3$ qubits the qMERA ansatz in Eq. (18) can also be represented as

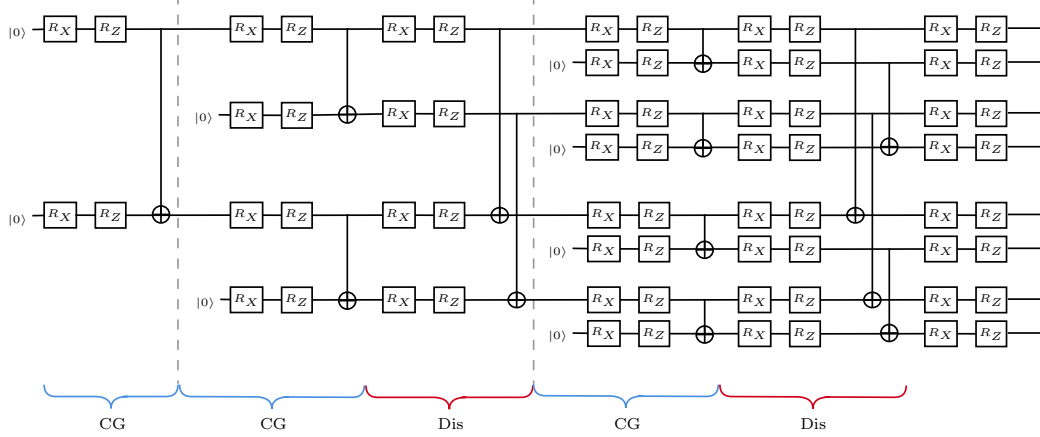


Figure 6: qMERA circuit considered in this article for $8 = 2^3$ qubits and 3 layers. For arbitrary $N = 2^n$ qubits and n layers, the l -th course-graining layer (CG in the figure) is as in the qTTN ansatz whilst the l -th disentangling layer is a composition of the $(l-1)$ -th disentangling layer with additional $R_X^{(j_1, j_2)} R_Z^{(j_1, j_2)} CNOT$ acting on adjacent pairs of the newly added qubits (j_1, j_2) within that layer (e.g. in the last disentangling operation above the last CNOT gates act on qubits (2, 4) and (6, 8) which were added on the last layer of the qMERA).

Note that this circuit is equivalent to the one presented in Eq. (18) up to a reordering of the qubits. The qubits in Fig. 6 are arranged so that the coarse-graining operations are equivalent to the ones in the qTTN PQC in Fig. 5. To that end we redefine the qMERA circuit as a product of course-graining and disentangling layers as

$$U^{\text{qMERA}} := \prod_{l=n}^1 U_l^{\text{DIS}} \cdot U_l^{\text{CG}}. \quad (\text{D1})$$

For all $l \geq 1$ the coarse-graining layers are

$$\begin{array}{c} \text{---} \\ \text{---} \\ \text{---} \\ \text{---} \end{array} \xrightarrow{U_l^{\text{CG}}} = \left. \begin{array}{c} \text{---} \\ \text{---} \\ \text{---} \\ \text{---} \end{array} \right|_{\substack{2^{n-l}-1 \\ 2^{n-l}-1}} \xrightarrow{\text{repeat}} \left. \begin{array}{c} \text{---} \\ \text{---} \\ \text{---} \\ \text{---} \end{array} \right|_{\substack{2^{n-l}-1 \\ 2^{n-l}-1}} \quad (\text{D2})$$

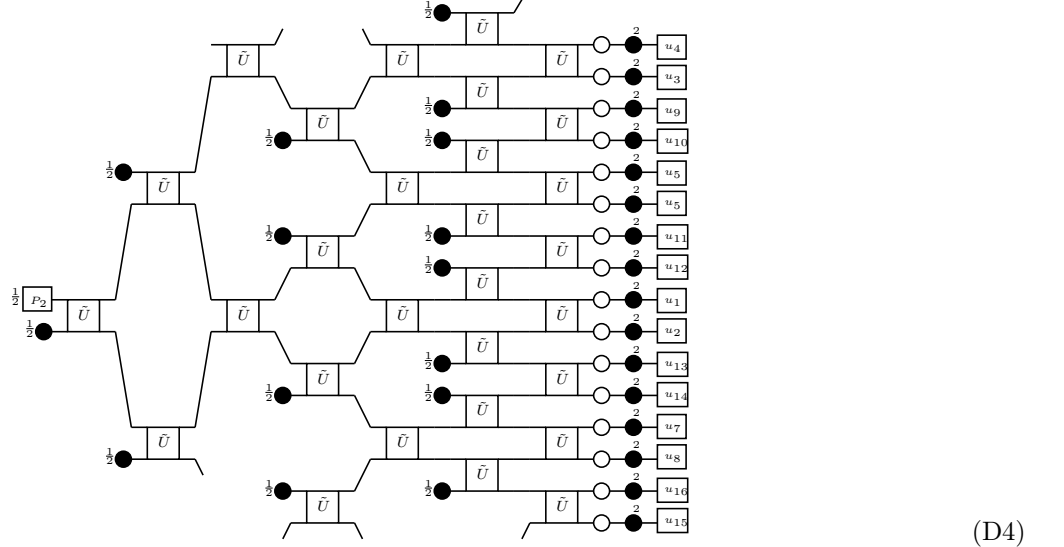
where the four registers are composed 2^{l-1} times in parallel (vertically). The disentangling layers are as follows: For $l=1$ $U_1^{\text{DIS}} = I$ and for $l \geq 2$

$$\begin{array}{c} \text{---} \\ \text{---} \\ \text{---} \\ \text{---} \end{array} \xrightarrow{U_l^{\text{DIS}}} = \left. \begin{array}{c} \text{---} \\ \text{---} \\ \text{---} \\ \text{---} \end{array} \right|_{\substack{2^{n-l} \\ 2^{n-l+1}-1 \\ 2^{n-l+1}-1}} \xrightarrow{\text{repeat}} \left. \begin{array}{c} \text{---} \\ \text{---} \\ \text{---} \\ \text{---} \end{array} \right|_{\substack{2^{n-l+1}-1 \\ 2^{n-l+1}-1}} \quad (\text{D3})$$

where the rotations and CNOT operation in the last 4 registers are repeatedly composed in parallel until $N = 2^n$ qubits are reached.

Back to the form in Eq. (D1), Theorem 2 and App. A imply that $\text{Var}[\partial_{1,1}\langle H \rangle_{\text{qMERA}}]$ for the 16 qubit qMERA

PQC in Eq. (D1) is given by the tensor network



where the vectors (and registers) are numbered according to the order in which they are added to the qMERA and where the matrix \tilde{U} is

$$\boxed{\tilde{U}} = \begin{array}{c} \text{---} \circ \text{---} \circ \text{---} \circ \text{---} \\ | \quad | \quad | \quad | \\ \text{---} \circ \text{---} \circ \text{---} \circ \text{---} \end{array} \quad (D5)$$

To calculate the variance for 1-local operators of the form X_i we replace $\mathbf{u}_i = \mathbf{v}_2$ and $\mathbf{u}_{i' \neq i} = \mathbf{v}_{13}$ and contract the resulting tensor network analytically. In general, this is an inefficient calculation.

We provide an alternative numerical method that exploits the structure of the qMERA and the causal cone of the observable X_i . In MERA the causal cone of a local observable has bounded width [69]. To lower-bound the variance of an observable X_i we want to choose the site i that leads to the widest causal cone. To upper-bound the variance we want to choose i leading to the narrowest causal cone. This is done to maximize (minimize) the number of qubit registers in the causal cone of X_i . Depending on the chosen site, the tensor network in Eq. (D4) can have a causal cone of width 2 or 3 as illustrated in Fig. 7 for sites 2 and 11 respectively. In general, one finds that the wider causal cones are found by choosing the registers that were added in the last course-graining layer of the qMERA (qubits 9 to 16 in the figure).

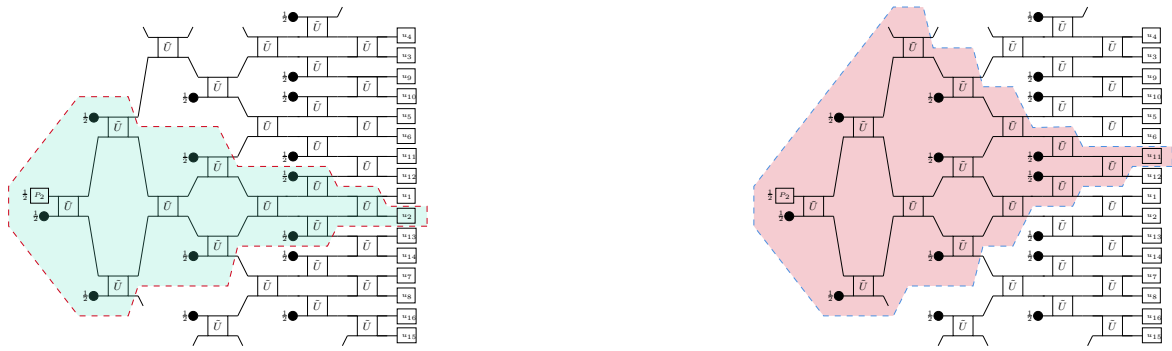
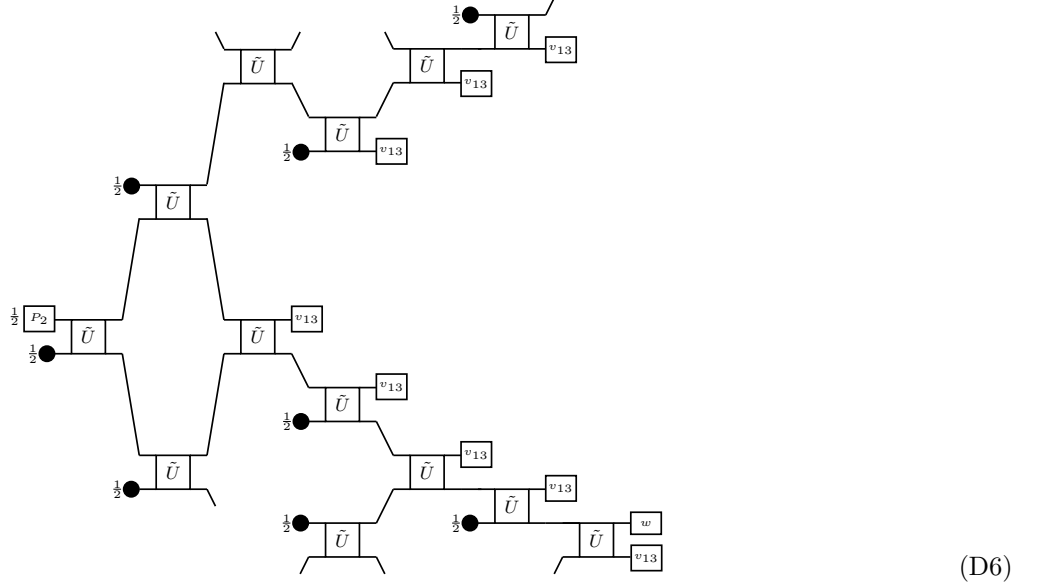


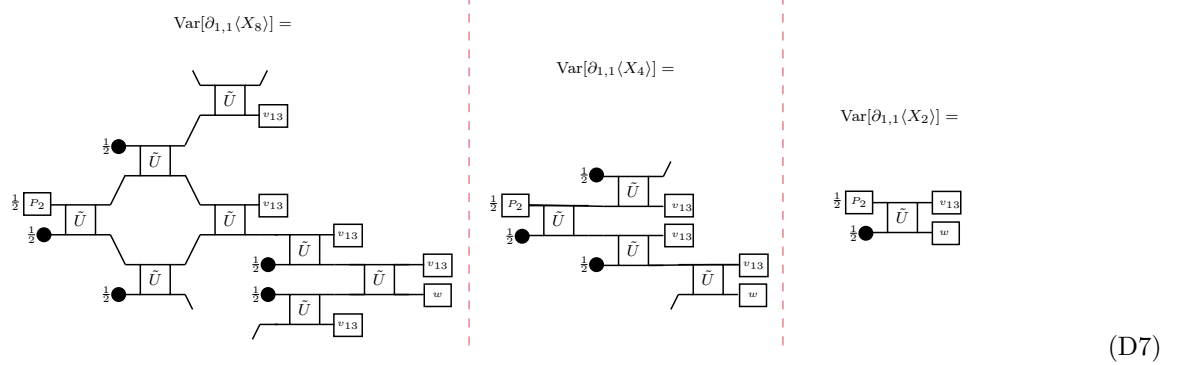
Figure 7: Causal cones for observables X_2 and X_{11} , respectively. The width of a causal cone is determined by the largest number of 2-qubit operations at any depth of the ansatz, e.g. the third course-graining layer of the causal cone on the right has three 2-qubit operations whereas the causal cone on the left never has more than two 2-qubit operations.

Using the arguments of Lemma 2 we choose observables X_N (X_1) for the ansatz in Fig. 6 to lower-bound (upper-bound) the gradient variance for one-local observables in qMERA. The respective variances are calculated by contracting the tensor network in Eq. (D4) numerically for 2, 4, 8, 16 qubits, taking care of choosing the correct sites

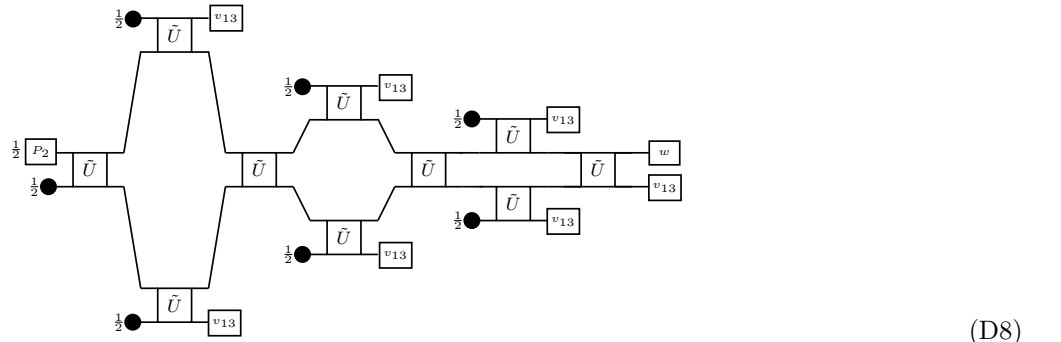
$i = 1, N$ as the ordering of qubits in the networks in Fig. 6 and Eq. (D4) differ. For the lower bound, $\text{Var}[\partial_{1,1}\langle X_{16} \rangle]$ is given by



where the vector $w = \frac{1}{2}(\mathbf{v}_2 + \mathbf{v}_{13}^-)$. In the cases of 8, 4, 2 qubits we have



For the upper bound, $\text{Var}[\partial_{1,1}\langle X_1 \rangle_{\text{qMERA}}]$ for 16 qubits is given by



and for 8, 4, 2 qubits by

$$\begin{aligned}
& \text{Var}[\partial_{1,1}\langle X_8 \rangle] = \\
& \quad \text{Circuit for } \text{Var}[\partial_{1,1}\langle X_8 \rangle] \\
& \text{Var}[\partial_{1,1}\langle X_4 \rangle] = \\
& \quad \text{Circuit for } \text{Var}[\partial_{1,1}\langle X_4 \rangle] \\
& \text{Var}[\partial_{1,1}\langle X_2 \rangle] = \\
& \quad \text{Circuit for } \text{Var}[\partial_{1,1}\langle X_2 \rangle]
\end{aligned} \tag{D9}$$

By contracting these networks, we find:

Claim 1. Let $\langle X_N \rangle_{qMERA}$ be the cost function associated with the observable X_N and consider the qMERA circuit defined in Eq. (D1), then:

$$\text{Var}[\partial_{1,1}\langle X_N \rangle_{qMERA}] \approx \begin{cases} 0.09375 \text{ for } N = 2 \\ 0.02477 \text{ for } N = 4 \\ 0.004109 \text{ for } N = 8 \\ 0.000622 \text{ for } N = 16 \end{cases}, \quad \text{Var}[\partial_{1,1}\langle X_1 \rangle_{qMERA}] \approx \begin{cases} 0.1719 \text{ for } N = 2 \\ 0.05242 \text{ for } N = 4 \\ 0.02304 \text{ for } N = 8 \\ 0.00882 \text{ for } N = 16 \end{cases} \tag{D10}$$

Looking at these results in a log-log plot we find that the data for $N = 4, 8$ and 16 lie on straight lines that give us the upper bound scaling like $O(N^{-1.2})$ and the lower bound scaling like $\Omega(N^{-2.7})$. The numerical results showcase a general brute-force approach to calculating the variances for the proposed qMERA for arbitrary 1-local observables.

To make a statement for general $N = 2^n$ qubits we argue as in Eq. (C23) using the tools from Lemma 2. Theorem 6 states that

$$\text{Var}[\partial_{1,1}\langle X_N \rangle_{qMERA}] \geq \text{Var}[\partial_{1,1}\langle X_{\hat{N}} \rangle_{qTTN}] = \frac{1}{4} \cdot \left(\frac{3}{8}\right)^{2 \log N} \tag{D11}$$

where $\hat{N} = 2^{2 \log N}$. Indeed the 1-local observable X_i in the qMERA circuit is causally connected to at most $2 \log N$ qubits. Lemma 2 suggests that, in the form of Fig. 6, the contributions are smallest when carried by the ‘up’ operation (C11). Hence $\text{Var}[\partial_{1,1}\langle X_i \rangle_{qMERA}]$ is lower-bounded by a circuit analogous to the one in Eq. (C2) but with $2 \log N$ qubits instead.

We use the same arguments for k -local observables of the form X_I acting on qubits $I = \{i_1, \dots, i_k\}$ for $k \ll N$ as in Conjecture 3. The observable X_I is causally connected to an upper bound of $2k \log N$ qubits and so:

$$\text{Var}[\partial_{1,1}\langle X_I \rangle_{qMERA}] \geq \text{Var}[\partial_{1,1}\langle X_{\hat{N}} \rangle_{qTTN}] = \frac{1}{4} \cdot \left(\frac{3}{8}\right)^{2k \log N} \tag{D12}$$

where $\hat{N} = 2^{2k \log N}$ by similar arguments as used at the end of App. C. These bounds are not tight, but as long as $k \ll N$ they still suggest that the qMERA avoids the barren plateau problem for k -local Hamiltonians. In the limit $k \approx N$ we obtain exponentially vanishing gradients as all qubits are in the causal cone of the observable.